AD-A083 039 STATE UNIV OF NEW YORK AT ALBANY F/G 20/6
THE EFFECT OF ATMOSPHERIC PARTICULATE MATTER ON THE PROPAGATION--ETC(U)
APR 80 P CHYLEK DAAG29-79-G-0031
UNCLASSIFIED ARO-16508.2-GS NL

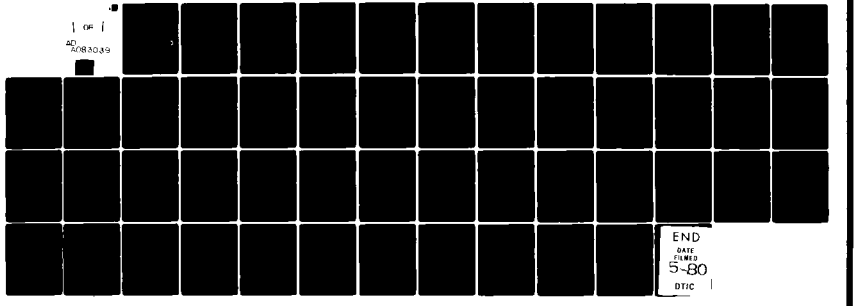

Unclassified

SECURITY CLASSIFICATION OF THIS PAGE (When Data Entered)

REPORT DOCUMENTATION PAGE

READ INSTRUCTIONS BEFORE COMPLETING FORM

1. REPORT NUMBER: 16508.2-GS	2. GOVT ACCESSION NO
3. RECIPIENT'S CATALOG NUMBER	
4. TITLE (and Subtitle): THE EFFECT OF ATMOSPHERIC PARTICULATE MATTER ON THE PROPAGATION OF A LASER BEAM.	5. TYPE OF REPORT & PERIOD COVERED: Final Report 1 Jan 79 — 31 Dec 79
	6. PERFORMING ORG. REPORT NUMBER
7. AUTHOR(s): Petr Chýlek	8. CONTRACT OR GRANT NUMBER(s): DAAG29-79-G-0031
9. PERFORMING ORGANIZATION NAME AND ADDRESS: University of New York, Albany, New York 12211	10. PROGRAM ELEMENT, PROJECT, TASK AREA & WORK UNIT NUMBERS
11. CONTROLLING OFFICE NAME AND ADDRESS: U. S. Army Research Office, P. O. Box 12211, Research Triangle Park, NC 27709	12. REPORT DATE: 11 Apr 80
	13. NUMBER OF PAGES: 48
14. MONITORING AGENCY NAME & ADDRESS (if different from Controlling Office)	15. SECURITY CLASS. (of this report): Unclassified
	15a. DECLASSIFICATION/DOWNGRADING SCHEDULE

ADA080339

LEVEL II

16. DISTRIBUTION STATEMENT (of this Report)

Approved for public release; distribution unlimited.

DTIC ELECTE APR 15 1980 D C

17. DISTRIBUTION STATEMENT (of the abstract entered in Block 20, if different from Report)

18. SUPPLEMENTARY NOTES

The view, pinions, and/or findings contained in this report are those of the author(s) and should not be construed as an official Department of the Army position, policy, or decision, unless so designated by other documentation.

19. KEY WORDS (Continue on reverse side if necessary and identify by block number)

light scattering
atmospheric particles
wave propagation
remote sensing
perturbation theory
electromagnetic waves
extinction cross sections
scattering cross sections

20. ABSTRACT (Continue on reverse side if necessary and identify by block number)

Perturbation Approach to Light Scattering by Nonspherical Particles: A series of calculations were performed, applying the first order perturbation theory to the scattering of electromagnetic waves by nonspherical particles. The numerical results obtained using the perturbation approach were compared with those using the extended boundary condition method. In this way the region of applicability of the first order perturbation method was established. 2. Light Scattering by a Pair of Conjugate Nonspherical Particles: Defining pair of conjugate non-

DD FORM 1473 EDITION OF 1 NOV 65 IS OBSOLETE

Unclassified 56550

SECURITY CLASSIFICATION OF THIS PAGE (When Data Entered)

20. ABSTRACT CONTINUED

spherical particles as a pair of particles that are a mirror image of each other and using the first order perturbation theory, it was learned that the sum of scattering or extinction cross sections of these two nonspherical particles is equal to a scattering (or extinction) cross section of a suitably defined sphere.

FINAL REPORT

PERIOD COVERED BY REPORT: Jan. 1 - Dec. 31, 1979

TITLE OF PROPOSAL: The Effect of Atmospheric Particulate Matter on the Propagation of a Lasar Beam

CONTRACT OR GRANT NUMBER: 16508 GS

NAMES OF INSTITUTION: State University of New York at Albany

AUTHOR OF REPORT: Dr. Petr Chýlek

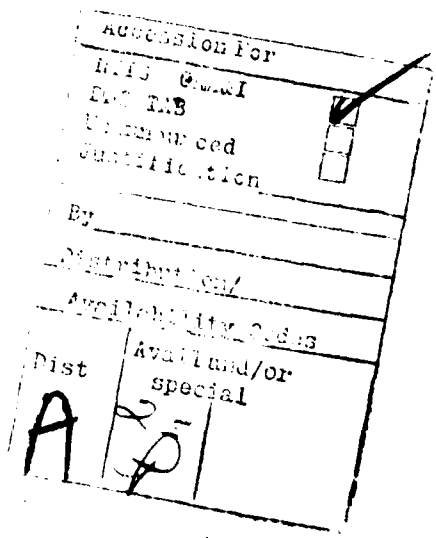

A. LIST OF PUBLICATIONS

1. P. CHÝLEK, J. KIEHL, A. MUGNAI: Light scattering by a pair of conjugate nonspherical particles. Journal of the Optical Society of America 69, 1550-1553 (1979).
2. R. PINNICK, G. JENNINGS, P. CHÝLEK, H. AUVERMANN: Verification of a linear relation between IR extinction, absorption and liquid water content of fogs. Journal of the Atmospheric Sciences 36, 1577-1586 (1979).
3. J. KIEHL, M. KO, A. MUGNAI, P. CHÝLEK: Perturbation approach to light scattering by non-spherical particles. To be published in the Proceedings of the Workshop on Light Scattering by Irregular Particles, Plenum Press, 1980.
4. P. CHÝLEK, J. KIEHL, M. KO, A. ASHKIN: Surface waves in light scattering by spherical and nonspherical particles. To be published in the Proceeding of the Workshop on Light Scattering by Irregular Particles, Plenum Press, 1980.

B. PARTICIPATING PERSONNEL

PETR CHÝLEK - Principal Investigator

J.T. KIEHL - Graduate Student

V. RAMASWAMY - Graduate Student

C. PROBLEM STUDIED

Light scattering by spherical and nonspherical particles and effect of scattering on atmospheric propagation and remote sensing.

D. MOST IMPORTANT RESULTS

1. Perturbation Approach to Light Scattering by Nonspherical Particles.

We have performed a series of calculations applying the first order perturbation theory to the scattering of electromagnetic waves by nonspherical particles. The surface of the nonspherical particle was parameterized in the form

$$r = r_s(1 + \varepsilon f(\theta,\phi)),$$

where r_s is a radius of unperturbed sphere, $f(\theta,\phi)$ describes the shape of nonspherical particles, and the perturbation parameters $\varepsilon << 1$. We have used several different forms of the shape function $f(\theta,\phi)$, and we have compared the numerical results obtained using the perturbation approach with those using the extended boundary condition method. In this way the region of applicability of the first order perturbation method was established.

2. Light Scattering by a Pair of Conjugate Nonspherical Particles.

We define a pair of conjugate nonspherical particles as a pair of particles that are a mirror image of each other. Using the first order perturbation theory we have learned that the sum of scattering or extinction cross sections of these two nonspherical particles is equal to a scattering (or extinction) cross section of a suitably defined sphere.

E. APPENDIX

Contains all papers supported by the ARO as listed in part A of the Report.

APPENDIX 1

Light scattering by a pair of conjugate nonspherical particles

Petr Chýlek,* J. T. Kiehl,* and A. Mugnai†

Center for Earth and Planetary Physics, Harvard University, Cambridge, Massachusetts 02138
and National Center for Atmospheric Research, Boulder, Colorado 80307

(Received 1 February 1979)

Applying the first-order perturbation theory, we have derived a theorem which states that, under specific conditions, the sum of the scattering matrices of two nonspherical particles can be replaced by the scattering matrix of a sphere. Consequently, a polydispersion of such nonspherical particles can be replaced by a polydispersion of spheres, without changing scattering characteristics of the polydispersion. This implies the nonuniqueness of the inverse-scattering problem. To verify the validity of the theorem, the differential scattering cross sections of several nonspherical rotationally symmetric particles have been calculated using the extended boundary condition method. The results show that the theorem is satisfied with accuracy expected from the first-order perturbation theory.

INTRODUCTION

Light scattering by small particles has found many applications in astronomy, biology, chemistry, meteorology, physics, and other branches of science. In some situations the scattering particles are spherical (for example, fog and cloud droplets) and in other situations they are nonspherical (dust particles in the Earth's or the Martian atmosphere, dust grains in interplanetary and intergalactic space, macromolecules, cells, etc.).

Because the scattering problem can be solved analytically only for very few highly symmetric shapes and because the analytical solution for spherical scatterers is much simpler than for other shapes, in many practical applications the Mie theory (scattering by spherical particles) is used regardless of the real shape of the scattering particles. Such a replacement of a nonspherical polydispersion of particles by a spherical polydispersion may be acceptable in some cases; however, in other cases it may lead to considerable discrepancies, depending on the exact shapes of the particles present. Unfortunately, there are no known criteria to decide under which conditions and with what accuracy nonspherical particles can be replaced by spherical particles. It is the purpose of this report to show that, under well-specified conditions, nonspherical particles can be replaced by spherical ones without significantly changing any of the scattering characteristics like scattering, absorption or extinction cross sections, differential scattering cross section, or the state of polarization of the scattered radiation.

CONJUGATE PARTICLES THEOREM

Consider for simplicity a nonspherical particle that can be obtained by the deformation of a sphere (Fig. 1) in such a way that the depth t of the layer in which the deformation occurs is equal to

$$t = 2r\epsilon, \tag{1}$$

where r is the radius of the original undeformed sphere and ϵ is a number considerably smaller than one. We should realize that even if

$$\epsilon \ll 1, \tag{2}$$

the thickness t does not have to be very small. For example, for $\epsilon = 0.1$, the thickness t is equal to 20% of the sphere's radius. It is convenient to parametrize the surface of such nonspherical particles by

$$r_s = r[1 + \epsilon f(\theta, \phi)], \tag{3}$$

where θ and ϕ are the usual spherical angular coordinates and the function $f(\theta, \phi)$ specifies the deviation of the particles from a sphere in the direction given by angles θ and ϕ.

Let us define what we will call a pair of nonspherical particles conjugate with respect to a sphere of radius r. Consider two nonspherical particles: particle A and particle B. If the surface of these two particles is described by the equations

$${}_Ar_s = r[1 + \epsilon f(\theta, \phi)], \tag{4}$$

$${}_Br_s = r[1 - \epsilon f(\theta, \phi)], \tag{5}$$

where ${}_Ar_s$ is the magnitude of the radius vector of an arbitrary point on the surface of particle A and ${}_Br_s$ is the magnitude of the radius vector of a surface point on particle B, we will say that the nonspherical particles A and B are conjugate with respect to a sphere of radius r. We can also say that the nonspherical particles A and B are conjugate with respect to a sphere of radius r if particle B is the mirror image of particle A with respect to a spherical mirror of radius r and vice versa. A few examples of conjugate nonspherical particles are shown in Fig. 2.

The electromagnetic field $\mathbf{E}_s$ scattered by a given particle (spherical or nonspherical) can be written in the form

$$\mathbf{E}_s = \mathbf{S}\,\mathbf{E}_i, \tag{6}$$

where $\mathbf{E}_i$ is the electric vector of the incoming radiation and $\mathbf{S}$ is a 2×2 scattering matrix, the form of which is determined by the properties of the scattering particle, such as the particle's shape, size, and material. To determine explicitly the form of the elements of the scattering matrix $\mathbf{S}$, one has to solve Maxwell's equations for the boundary conditions satisfied on the surface of the scattering particle; closed form analytical solutions have been derived only for spherical particles,[1] spheroids,[2] and infinitely long cylinders,[3] and it is doubtful that a closed form analytical solution can exist for an arbitrarily shaped particle as considered in this study.

Since the parameter ϵ appearing in Eqs. (3)–(5) is considerably smaller than one, however, first-order perturbation theory can be applied to the considered case of light scattering by nonspherical particles. It follows[4,5] that if light scattering

 0030-3941/79/111550-04$00.50

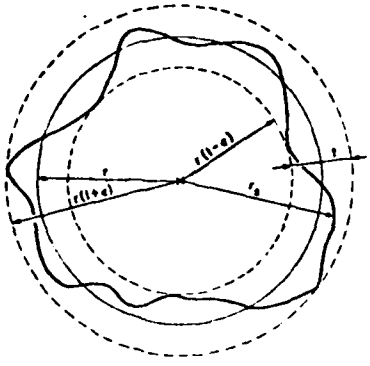

FIG. 1. Consideration of a nonspherical particle whose deviation from a sphere of radius r occurs only in a spherical shell of thickness t with inner and outer radius equal to $r(1-\epsilon)$ and $r(1+\epsilon)$, respectively.

by a spherical particle is described by the scattering matrix $\mathbf{S}$, then the scattering by a nonspherical particle A, as specified by Eq. (4), is described by the scattering matrix

$$_A\mathbf{S} = \mathbf{S} + \epsilon\,\mathbf{S}_1, \tag{7}$$

where the matrix $\mathbf{S}_1$ is independent of ϵ. Since the difference in the mathematical description of nonspherical particles conjugate to each other with respect to a sphere of radius r is only the sign of the parameter ϵ [compare Eqs. (4) and (5)], the scattering matrix $_B\mathbf{S}$ describing light scattering by a particle B (which is conjugate to A with respect to a sphere of radius r) is given by

$$_B\mathbf{S} = \mathbf{S} - \epsilon\mathbf{S}_1. \tag{8}$$

By adding Eqs. (7) and (8), we obtain a basic theorem—which we will call the conjugate particles theorem—allowing us to replace conjugate nonspherical particles by spherical particles without changing the observable scattering characteristics of the system. We obtain

$$_A\mathbf{S} + {}_B\mathbf{S} = 2\,\mathbf{S}, \tag{9}$$

which says that the sum of the scattering matrices of two nonspherical particles A and B, conjugate with respect to a sphere of radius r, is equal to twice the scattering matrix of a sphere of radius r.

Since $\epsilon \ll 1$, the same additive property is valid for experimentally observable quantities like the differential scattering cross section (phase function), absorption, scattering and extinction cross sections, and polarization (we neglect terms proportional to ϵ^2 and higher powers of ϵ).

Remember that the sum $_A\mathbf{S} + {}_B\mathbf{S}$ in Eq. (9) means the sum of two single-particle scattering matrices (not a two-particle scattering matrix). Also, we consider the case of incoherent scattering where distances between individual particles are much larger than the wavelength of the scattered radiation. Therefore, the sum $_A\mathbf{S} + {}_B\mathbf{S}$ is not a function of the distance between particles A and B.

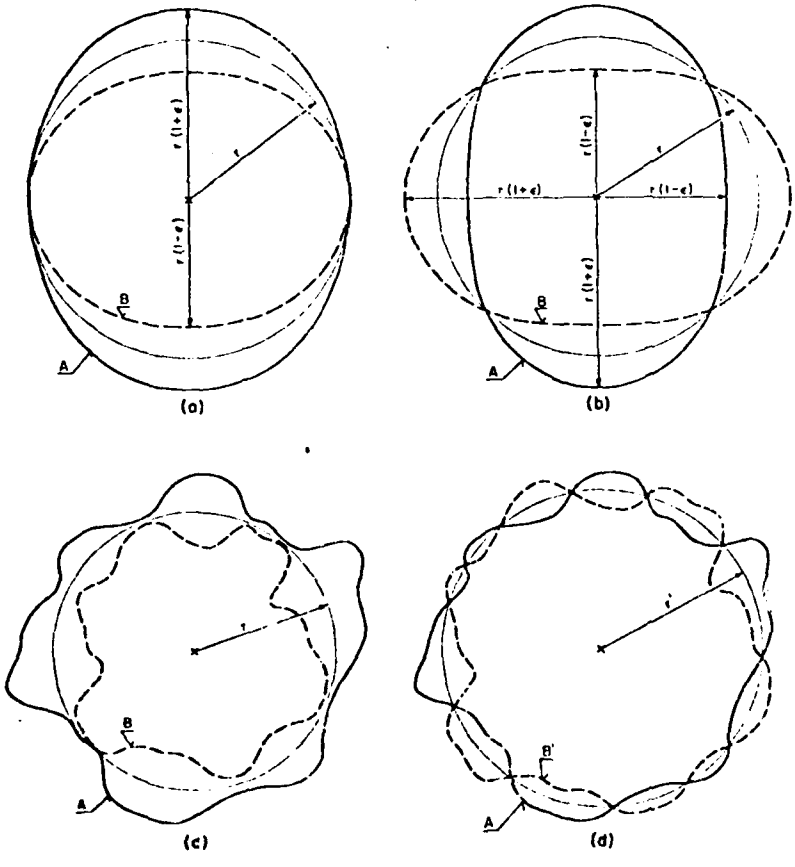

FIG. 2. Several examples of conjugate nonspherical particles. Nonspherical particles A (solid line) and B (dashed line) are conjugate with respect to a sphere of radius r. Particles shown in (a) and (b) are rotationally symmetric and resemble prolate and oblate spheroids very closely. To a given nonspherical particle A, the conjugate particle can be either a particle B or a particle B' depending on the radius of the sphere with respect to which the particles are conjugate [(c), (d)].

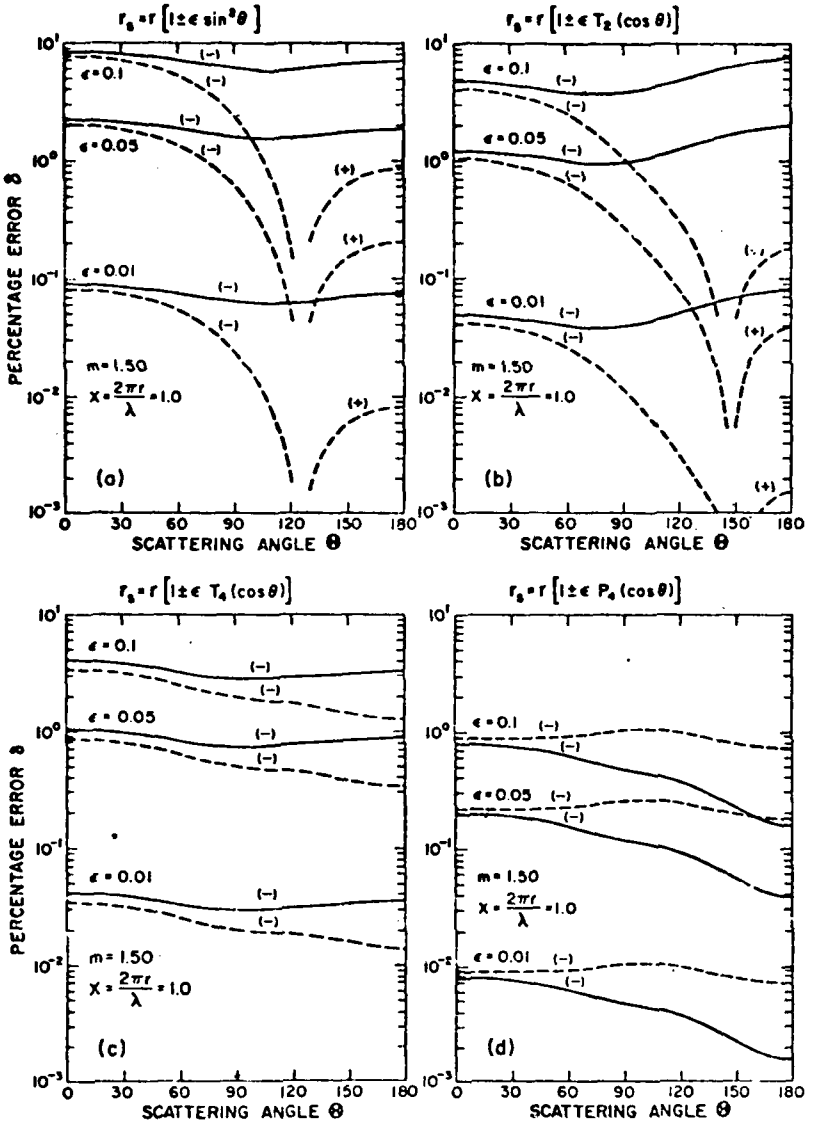

FIG. 3. Equation (11) satisfied with an error δ [Eq. (12)] for considered four pairs of conjugate nonspherical particles in Eqs. (10a)–(10d). For $\epsilon = 0.01$ the error in all cases is smaller than 0.1%. For $\epsilon = 0.1$, the error is smaller than 10%. In cases (a) and (b) the error δ changes the sign. In all cases an absolute value of δ is plotted and the corresponding parts of the curves are denoted by the (+) and (−) signs. The solid curves show the error for the case when particles are oriented in such a way that their axis of rotation is parallel to the direction of the incoming light, and the dashed curves show δ for the case of perpendicular orientation (axis of rotation perpendicular to the direction of the incoming light and perpendicular to the scattering plane chosen to be the x-z plane). The incoming radiation is propagating in the direction of the positive z axis and is linearly polarized with the electric vector making an angle of 45° with the x axis.

NUMERICAL RESULTS

To verify the validity of the derived theorem, we have calculated the differential scattering cross sections of several nonspherical axially symmetric particles using the extended boundary condition method.[6,7] We considered four sets of nonspherical conjugate particles given by the equations

$$r_s = r[1 \pm \epsilon \sin^2\theta], \tag{10a}$$

$$r_s = r[1 \pm \epsilon T_2(\cos\theta)], \tag{10b}$$

$$r_s = r[1 \pm \epsilon T_4(\cos\theta)], \tag{10c}$$

$$r_s = r[1 \pm \epsilon P_4(\cos\theta)], \tag{10d}$$

where $T_n(\cos\theta)$ is the nth Chebyshev polynomial of the first kind, and where $P_4(\cos\theta)$ is the fourth-order Legendre polynomial. While (10a) and (10b) are convex, particles described by Eqs. (10c) and (10d) are concave. Cross sectional views of the particles (10a) and (10b) are schematically shown on Figs. 2(a) and 2(b). Let us consider the relation between the differential scattering cross sections of the form

$$A\sigma + B\sigma = 2_r\sigma \tag{11}$$

following from the theorem [Eq. (9)] for the case $\epsilon \ll 1$ (in the above notation $_r\sigma$ stands for the differential scattering cross section of a sphere of radius r). In Fig. 3 the percentage error

$$\delta = \frac{2_r\sigma - (A\sigma + B\sigma)}{A\sigma + B\sigma} \times 100\% \tag{12}$$

is plotted as a function of the scattering angle for two different orientations of the scattering particles. In general, we can say that for $\epsilon = 0.01$ (deviation from a sphere occurs in an outer layer of thickness equal to 2% of the radius), the theorem is satisfied with an accuracy better than 0.1%. With $\epsilon = 0.05$ (t equal to 10% of the radius), the accuracy is than 2%; and finally with $\epsilon = 0.10$ (t equal to 20% of the radius), the accuracy is always better than 10%. This accuracy is in agreement with what one should expect from neglecting terms proportional

to ϵ^2 with respect to ϵ. We conclude that the numerical results confirm the validity of the conjugate particles theorem.

APPLICATIONS

The derived theorem has several practical consequences. Whenever we have a polydispersion of nonspherical particles such that for each nonspherical particle of the polydispersion there exists another nonspherical particle in the same polydispersion that is conjugate to the previous one with respect to a sphere of radius r, then the considered polydispersion of nonspherical particles can be replaced by a polydispersion of spheres (each pair of nonspherical particles conjugate with respect to a sphere of radius r is replaced—according to the theorem—by two spheres of radius r) without a change of scattering characteristics of the polydispersion. It means that within the accuracy of order ϵ all scattering characteristics of both polydispersions are identical and there is no experimental measurement that can distinguish between these two polydispersions on the basis of their scattering properties. This shows directly the nonuniqueness of the inverse-scattering problem. From the scattering characteristics measured with a definite experimental error we cannot deduce unambiguously the size distribution of the scattering particles (even if we assume that the index of refraction is known). Even more, we are not able to determine whether particles are spherical or nonspherical. Of course, with increasing experimental accuracy the range of ambiguity decreases.

If a nonspherical particle is self-conjugate (conjugate to itself in a different orientation) with respect to a sphere of radius r, then the scattering matrix of this particle averaged over all orientations is equal to the scattering matrix of a sphere of radius r.

If we write the conjugate particles theorem of Eq. (9) in the form

$$_B\mathbf{S} = 2\,\mathbf{S} - {}_A\mathbf{S}, \tag{13}$$

we can see that the scattering matrix of the nonspherical particle B can be calculated once we know the scattering matrix of the nonspherical particle A conjugate to B with respect to a sphere of radius r. Let us assume that the scattering matrix of the nonspherical particle A is known. We can make, for example, a model of the particle A and perform microwave scattering experiments to determine its scattering matrix. Then we can choose a set of spheres with radii r_1, r_2, r_3, . . . , r_i and determine the shapes of the nonspherical particles B_1, B_2, . . . , B_i conjugate to the nonspherical particle A with respect to the spheres of radii $r_1, r_2, r_3, \ldots, r_i$. Then the scattering matrices for the nonspherical particles B_1, B_2, B_3, . . . , B_i can be calculated from Eq. (13). Thus, one experimental measurement can provide scattering matrices for several differently shaped nonspherical particles.

Finally, one can similarly define nonspherical particles conjugate with respect to a surface other than a sphere (for example, with respect to an oblate or a prolate spheroid) and then replace a polydispersion of irregular conjugate particles by a polydispersion of spheroidal particles the scattering property of which can be calculated analytically.

ACKNOWLEDGMENTS

This research was supported in part by the U.S. Army Research Office, by the Atmospheric Research Section of the National Science Foundation, and by Piani Finalizzati-Consiglio Nazionale delle Ricerche of Italy. The authors wish to thank Dr. P. Barber for providing them with a computer program for the extended boundary condition method. The National Center for Atmospheric Research is sponsored by the National Science Foundation.

*On leave from the Atmospheric Science Research Center and Department of Atmospheric Science, State University of New York, Albany, New York 12222.

†On leave from CNR-LPS Elettrofisica Atmosferica, Frascati, Italy.

[1] G. Mie, "A contribution to the optics of turbid media, especially colloidal metallic suspensions," Ann. Phys. 25, 377–445 (1908).

[2] S. Asano and G. Yamamoto, "Light scattering by a spheroidal particle," Appl. Opt. 14, 29–49 (1975).

[3] J. R. Wait, "Scattering of a plane wave from a circular dielectric cylinder at oblique incidence," Can. J. Phys. 33, 189–195 (1955).

[4] C. Yeh, "Perturbation approach to the diffraction of electromagnetic waves by arbitrarily shaped dielectric obstacles," Phys. Rev. 135, A1193–A1201 (1964).

[5] V. Erma, "Exact solution for the scattering of electromagnetic waves from bodies of arbitrary shape," Phys. Rev. 179, 1238–1246 (1969).

[6] P. C. Waterman, "Symmetry, unitarity and geometry in electromagnetic scattering," Phys. Rev. D 3, 825–839 (1971).

[7] P. Barber and C. Yeh, "Scattering of electromagnetic waves by arbitrarily shaped dielectric bodies," Appl. Opt. 14, 2864–2872 (1975).

APPENDIX 2

Reprinted from JOURNAL OF THE ATMOSPHERIC SCIENCES, Vol. 36, No. 8, August 1979
American Meteorological Society
Printed in U. S. A.

Verification of a Linear Relation between IR Extinction, Absorption and Liquid Water Content of Fogs

R. G. PINNICK

U.S. Army Atmospheric Sciences Laboratory, White Sands Missile Range, NM 88002

S. G. JENNINGS[1]

Department of Pure and Applied Physics, University of Manchester Institute of Science and Technology, Manchester, England

PETR CHÝLEK

Center for Earth and Planetary Physics, Harvard University, Cambridge, MA 02138

H. J. AUVERMANN

Physical Sciences Laboratory, New Mexico State University, Las Cruces, NM 88003

(Manuscript received 15 December 1978, in final form 3 April 1979)

ABSTRACT

A linear relationship, independent of the form of the size-distribution, between extinction at wavelengths around $\lambda = 11\ \mu m$, absorption around $\lambda = 3.8$ and $9.5\ \mu m$, and liquid water content of atmospheric fogs has been verified using 341 droplet size distribution measurements made under a variety of meteorological conditions. The results suggest that integrated liquid water content along a path in fog can be determined from measurement of CO_2 laser ($\lambda = 10.6\ \mu m$) transmission along the path, and that liquid water content at a particular point in fog can be inferred from *in situ* measurement of fog-droplet absorption with a deuterium fluoride laser ($\lambda = 3.8\ \mu m$) or a suitably tuned CO_2 laser ($\lambda = 9.5\ \mu m$) spectrophone.

1. Introduction

It has been recently shown (Chýlek, 1978) that a linear relationship, independent of the form of the size distribution, should exist between the infrared extinction around $\lambda = 11\ \mu m$ and the liquid water content of fogs. The relation can be written in the form

$$\sigma_e = \frac{3\pi c}{2\rho\lambda} W, \tag{1}$$

where σ_e is the volume extinction coefficient measured at the wavelength λ, W the liquid water content, ρ the density of water, and the coefficient c is equal to the slope of a straight line that approximates the extinction efficiency curve $Q_e(x,\lambda)$ by

$$Q_e(x,\lambda) = c(\lambda)x, \tag{2}$$

where the size parameter x is defined by the ratio of the particle circumference to the wavelength. An approximate value of the coefficient $c(\lambda)$ at $\lambda = 11\ \mu m$ is $c \approx 0.31$. The conditions under which the approximation (2) are valid and the derivation of the relation (1) have been discussed elsewhere (Chýlek, 1978).

In this paper we verify the validity of relation (1) by calculating the volume extinction coefficient σ_e and the liquid water content W for 341 different fog droplet size distributions (Garland, 1971; Kumai, 1973; Garland *et al.*, 1973; Kunkel, 1971; Roach *et al.*, 1976; Pinnick *et al.*, 1978) measured under various meteorological situations.

We also show that a linear relationship, similar to (1), exists between the infrared absorption coefficient in the spectral regime $\lambda = 3.5$–$5.3\ \mu m$, 8–$10\ \mu m$, and the liquid water content of fogs. Thus for example, the absorption coefficient of fogs at $\lambda = 3.8\ \mu m$ is uniquely related to their extinction and absorption at $\lambda = 10\ \mu m$.

2. Selected fog size distributions

Relatively few reliable measurements of fog droplet size distributions have been made, particu-

[1] Visiting U.S. Army Atmospheric Sciences Laboratory.

0022-4928/79/081577-10$06.50

FROM

larly for which numerical data are available. The fog measurements used here we judge to be reliable and were chosen to represent a wide range of fog conditions ranging from maritime and continental advection fogs [Kumai, 1973; Kunkel, 1971; and part of Garland's (1971) work] to inland radiation fogs (Garland, 1971; Garland *et al.*, 1973; Roach *et al.*, 1976; Pinnick *et al.*, 1978). The early work on evolving fogs near the Atlantic Ocean in France and stable inland fog and haze near Paris by Arnulf *et al.* (1957) was not used because it was not possible to obtain true droplet distributions from their figures. Arnulf *et al.* (1957) captured droplets on spider threads (for which the capture coefficient depends on droplet size) but gives only the uncorrected droplet distribution data. Results of the pioneering work of May (1961) using a specially designed two-stage impactor were not used since the numerical data are no longer available (May, private communication, 1978). Measurements of valley fog drop sizes obtained by exposing gelatin-coated slides to a stream of foggy air by Pilié *et al.* (1975) were deemed not credible since the distributions were normalized to simultaneous measurements of extinction coefficient derived by a transmissometer. Fog drop measurements made with a light-scattering counter by Eldridge (1961) were not utilized since we suspect errors in his measurements due to non-isokinetic sampling. The inlet of his counter was only 1 cm in diameter and became wet during the sampling process. In addition, some unexplained differences were caused by a dilution apparatus Eldridge used for high droplet concentration conditions.

Three different sampling techniques were employed to obtain the fog size distributions utilized in this study: impaction, holographic and light scattering.

Garland (1971), Garland *et al.* (1973) and Roach *et al.* (1976) used a modified two-stage Casella impactor designed by May (1961) mounted horizontally in a wind tunnel to provide isokinetic sampling. Corrections to the collection efficiency based on the penetration curves of the impactor (May, 1945) were applied to the raw data. This device is sensitive to droplets of 3–72 μm radius.

Kumai (1973) also used a two-stage impactor to measure advection fog droplets formed over the Arctic Ocean at Point Barrow, Alaska, together with a gelatin-coated glass collection plate whose collection efficiency was available as a function of wind velocity. Also, droplet correction factors were applied to true sizes. The combined methods yielded droplet concentration from 2.2–64 μm radius.

In general, the primary disadvantage of the impaction technique, besides requiring laborious data reduction, is the uncertainty in droplet concentration determination for near and submicrometer size droplets. In addition, the size limit of detectability is about 0.3 μm radius using conventional microscopy techniques.

A laser hologram technique was employed by Kunkel (1971) to measure droplets in advection fog propagating inland during nighttime at Otis Air Force Base, Massachusetts. The hologram camera was capable of sampling volumes of 4.5 cm^3 at a rate of five samples per minute, in a near-isokinetic fashion, and with minimal disturbance to the droplets. Droplets with radius 2–40 μm were detected. Because of the small number of droplets (normally <50) in the distributions reported by Kunkel, we have averaged all 17 of the reported droplet distributions together, which in any case represents only a 3-min interval, to obtain a single distribution.

Finally, we have used measurements by Pinnick *et al.* (1978) of radiation fog and haze made during wintertime in West Germany with a commercially available light-scattering counter (the "Knollenberg" Classical Scattering Aerosol Spectrometer manufactured by Particle Measurement Systems, Boulder, Colorado). This device works on the principle that as aerosol flows through an illuminated volume, light scattered by single droplets into a particular solid angle is measured and used to determine particle size by making pulse-height analyses of the response pulses. Determination of droplet size from the response is indirect because of the dependence of the response on factors other than droplet size, viz., droplet refractive index and the lens geometry of the optical system. Particular attention was given to the calibration of this instrument using monodisperse particles of different size and refractive index. The manufacturer's advertised calibration was not used. Rather, droplet size distributions were determined by redefining the size pulse-height channels as described in detail by Pinnick *et al.* (1978). This counter is sensitive to water droplets with radii 0.23–16 μm.

Altogether, 341 different size distributions were used to check the validity of Eq. (1) in the atmospheric window around $\lambda = 11$ μm; 25 fog distributions were taken from Garland (1971) and Roach *et al.* (1976), 6 from Garland *et al.* (1973), 20 from Kumai (1973), 1 from Kunkel (1971), and 289 fog and haze distributions from Pinnick *et al.* (1978).

3. Numerical results for fog extinction

Using a Mie scattering program and index of refraction of water as given by Hale and Querry (1973), we have calculated the volume extinction coefficient

$$\sigma_e(\lambda) = \pi \int r^2 Q_e(\lambda, r) n(r) dr \qquad (3)$$

and the liquid water content

$$W = \tfrac{4}{3}\pi\rho \int r^3 n(r) dr \qquad (4)$$

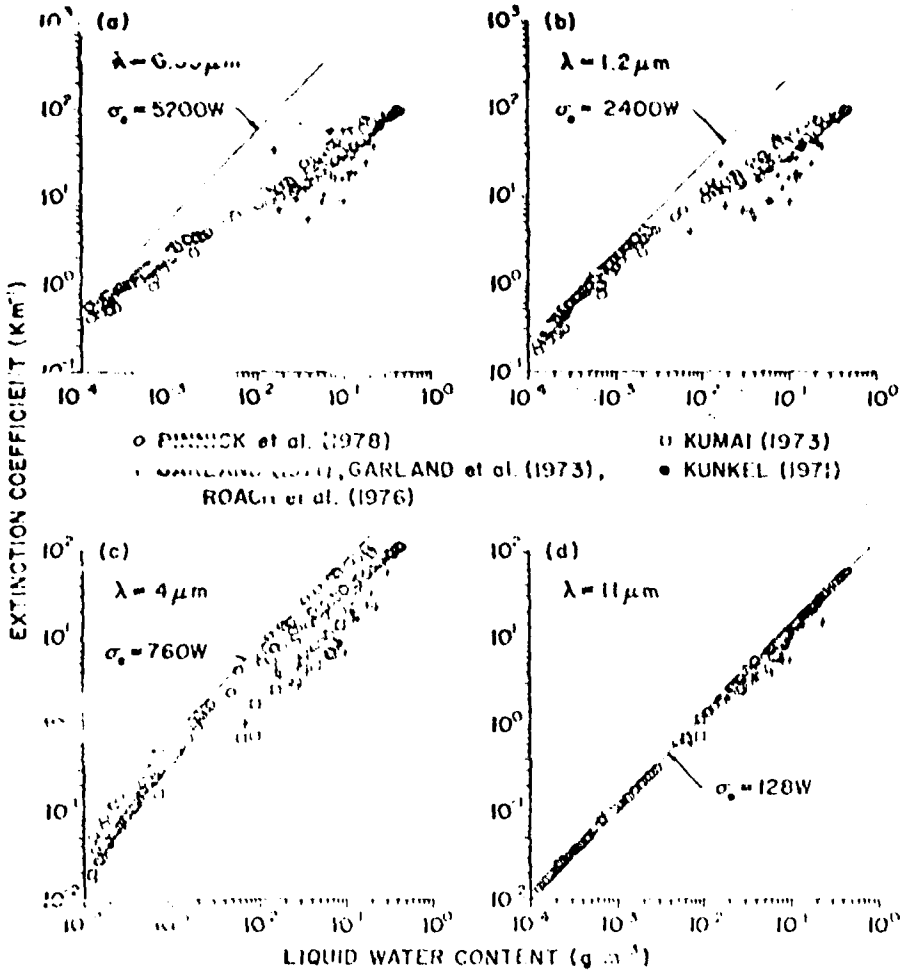

FIG. 1. Variation of extinction coefficient with liquid water content in atmospheric fog and haze for 341 size distribution measurements made at different geographic locales and under a variety of meteorological conditions. In the infrared spectral region around $\lambda = 11$ μm (d) there exists a linear, size distribution independent relation between the volume extinction coefficient σ_e(km^{-1}) and the liquid water content W (g m^{-3}) of the form of Eq. (1). Consequently, the results of all measurements are close to a straight line. The predicted relation between extinction σ_e and liquid water content W according to Eq. (1) is shown by the straight line. On the other hand at $\lambda = 0.55$ μm (a), the $Q_{ext} = 2$ approximation is not satisfied and no unambiguous relation between extinction and liquid water content exists. The large spread of the points in the graph shows that the extinction coefficient is a function of the size distribution as well as of the liquid water content. As the wavelength is increased to $\lambda = 1.2$ μm (b) and $\lambda = 4$ μm (c) the $Q_{ext} = 2$ approximation is established for larger droplets and the relation (1) shown by the straight lines is becoming a more realistic approximation for hazes and fogs.

for the previously mentioned 341 fog and haze size distributions $n(r)$ at several different wavelengths λ. The numerical integrations were performed only over the range of particle radii measured for each size distribution, under the assumption that the differential size distribution $n(r)$ is constant within each measured particle size channel. In other words, there was no extension of the measured distributions to larger or smaller particle sizes and no smoothing of the measured distributions. The results at $\lambda = 0.55$, 1.2, 4 and 11 μm, together with the $Q_{ext} = 2$ approximation [Eq. (1)] are shown in Fig. 1. We have not included the Kumai (1973) or Kunkel (1971) results at $\lambda = 0.55$ μm, 1.2 μm since we suspect the contribution of particles with $r > 2$ μm (which neither Kumai nor Kunkel measured) to extinction at these wavelengths might be excessive.

At $\lambda = 11$ μm the $Q_{ext} = 2$ approximation is a good approximation for all size distributions except those with a large number of droplets with radii $r > 14$ μm (Chylek, 1978). Some fog size distributions used in our calculations contained droplets

with $r > 14$ μm; however, their contribution generally did not dominate either the extinction σ_e or the liquid water content W. Consequently, we expect that the linear relationship (1) between the volume extinction coefficient σ_e and the liquid water content W will be reasonably well satisfied at $\lambda = 11$ μm. Results of numerical calculations confirming the validity of Eq. (1) at $\lambda = 11$ μm are shown in Fig. 1d.

On the other hand at $\lambda = 0.55$ μm the approximation $Q_e = cx$ is valid only for water droplets with $r \leq 0.5$ μm (Chýlek, 1978). Since most haze and all fog droplet size distributions are dominated by droplets with $r > 0.5$ μm, the $Q_e = cx$ approximation is not valid in this case and, consequently, no size-distribution-independent relation between the extinction and liquid water content should exist at $\lambda = 0.55$ μm. The numerical results based on the measured distributions compared to the Eq. (1) approximation in Fig. 1a confirm this conclusion. Further, the approximation grossly overestimates extinction for most of the distributions.

As we change the wavelength from $\lambda = 0.55$ μm to longer wavelengths, the $Q_e = cx$ approximation is satisfied for larger droplet radii. Consequently, with increasing wavelength the relation given by Eq. (1) is becoming a more realistic approximation for hazes and for fogs. This trend can be seen from Figs. 1b–1c, showing the numerical calculations and the Eq. (1) approximation at $\lambda = 1.2$ and 4 μm. We note that with increasing λ the relation (1) better approximates the exact numerical results and finally at $\lambda = 11$ μm (Fig. 1d) the volume extinction coefficient becomes independent of the size distribution $n(r)$, and the relation (1) agrees within a factor 2 with the numerical results for all distributions.

Closer inspection of the results in Fig. 1d shows noticeably better agreement between the Mie numerical results and the relation (1) for the size distributions of Pinnick *et al.* (1978). The reason very likely has to do with the fact that the size distribution measurements of Pinnick *et al.* are only for droplets with radii up to $r = 16$ μm, whereas the Garland (1971), Garland *et al.* (1973) and Roach *et al.* (1976) measurements are for droplets with radii up to $r = 72$ μm; the Kunkel (1973) measurements are for droplets with radii up to $r = 64$ μm; and the Kunkel (1971) measurement is for droplets with radii up to $r = 40$ μm. Since the maximum radius condition for the $Q_e = cx$ approximation leading to relation (1) is for $r \approx 2$ μm at $\lambda = 11$ μm, none of the Pinnick *et al.* distributions can strongly violate this condition since particles with $r > 16$ μm were measured. Also the better agreement of the numerical results for the Pinnick *et al.* distributions with the relation (1) at $\lambda = 11$ μm [and also at $\lambda = 4$ μm (see Fig. 1c)] may be in part a consequence of their inability to measure droplets with $r > 16$ μm.

Another qualification concerning the results in Fig. 1 bears on our assumption that all fog and haze particles consist of homogeneous water droplets and have complex refractive indexes of water. Haze particles in particular may contain a significant volume fraction of contaminants such as sea salt or ammonium sulfate. The crucial question here is to what degree is the particle refractive index affected by such contaminants? We know in the case of fog that its formation requires atmospheric relative humidity RH to be near 100%. We also know that for the haze data appearing in Fig. 1 the relative humidity was close to 100% (Pinnick *et al.*, 1978). Hänel (1976) and Hänel and Bullrich (1978) have studied the effect of relative humidity variations on mean complex refractive indexes of maritime and urban aerosols. Hänel (1976) found that for RH $\geq$ 95% the real and imaginary parts of the complex refractive index n_{re} and n_{im} at $\lambda = 0.55$ μm have values $1.33 \leq n_{re} \leq 1.36$, $0 \leq n_{im} \leq 0.006$. Examination of Mie efficiency factors $Q_e(m,x)$ for refractive indexes in this range shows our assumption that $m = 1.33-0i$ in Mie calculations of extinction according to (3) and the $Q_e = cx$ approximation (1) is a good one. At wavelengths $>\lambda = 0.55$ μm we find from Hänel and Bullrich's formulas for values of RH $>$95% that both maritime and urban aerosol mean refractive indexes are again not markedly different from those of water. For example, at $\lambda = 11$ μm we predict from Hänel and Bullrich's formulas that the real and imaginary parts of the complex index are $1.153 \leq n_{re} \leq 1.207$, $0.0968 \leq n_{im} \leq 0.109$, compared to $m = 1.153-0.0968i$ for pure water. The effect of these refractive index variations in Mie calculations of extinction coefficient according to (3) and (1) are estimated to be not more than 10%. For fog, an additional argument can be made to support our assumption that the particle refractive indexes can be approximated by those of pure water. The argument is that the liquid mass content of fogs is on the order of 0.005 g m^{-3} or greater, and thus the volume fraction of any contaminant in fog droplets must necessarily be small so that the refractive indexes must be close to those of water.

In order to examine more closely the fog results in Fig. 1 in terms of fog type we have chosen to restrict our attention to the data of Garland (1971), Garland *et al.* (1973) and Roach *et al.* (1976). The reasons are twofold: first, these measurements were made during fogs occurring under distinctly different meteorological conditions. Altogether, 37 different fogs were measured during a five-year period under the gamut of meteorological conditions found in England. Second, measurements were made for a

sufficiently broad range of particle sizes (0.3 μm $< r <$ 72 μm) that errors in extinction and liquid water content due to the presence of larger and smaller droplets are estimated to be small. Of the 37 measured distributions, three were not used due to nonavailability of the raw data, three because of the presence of ice crystals in the samples, and five were not used because fog type was not specified.

We have divided the Garland and Roach *et al.* fog data, which already appear in Fig. 1, into two classes: radiation fog and advection fog. We have been cautioned (Garland, private communication, 1978) that although the radiation fogs clearly formed *in situ* by radiation cooling, some fogs classified as advection type may have been mature radiation fogs transported by the wind from a distant area of formation. In any case, the data are replotted according to this classification in Fig. 2 (λ = 0.55 μm) and Fig. 3 (λ = 11 μm). At λ = 0.55 μm it is evident radiation fogs are generally more effective scatterers, and hence more effective in reducing visibility, than advection fogs with the same liquid water content. To understand the reason for this result, we have picked a radiation fog (Fig. 2, solid circle) and an advection fog (Fig. 2, solid square) measurement with about the same liquid water content, and have plotted their differential extinction coefficients at λ = 0.55 μm vs particle radius in Fig. 4. Because the plots are made on a linear scales, the areas under the curves are a measure of the corresponding extinction coefficients. Thus the radiation fog extinction coefficient (25 km^{-1}) is more than twice the advection fog extinction coefficient (15.8 km^{-1}). For the radiation fog, small droplets, say, $r \leq 3$ μm, are very numerous and contribute 60% of the extinction without making a significant contribution to liquid water content. On the other hand, for advection fog, a broader size distribution is found and these smaller particles contribute only 6% of the extinction at λ = 0.55 μm. Both the radiation and the advection fog size distributions strongly violate the maximum radius condition allowed in the $Q_e = cx$ approximation (r_m = 0.5 μm at λ = 0.55 μm), so there is no reason to expect a unique relation between extinction at λ = 0.55 μm and liquid water content.

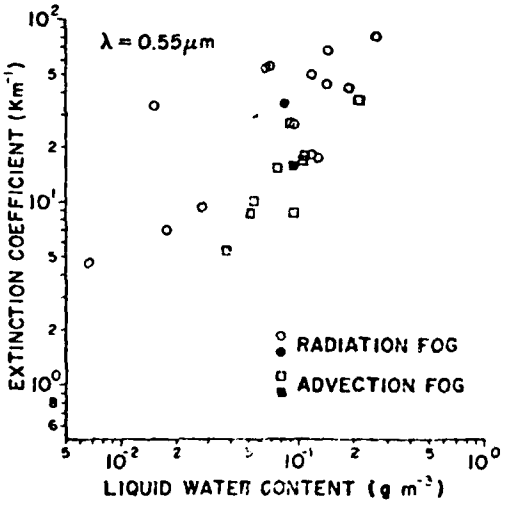

FIG. 2. As in Fig. 1a except that only the fog data of Garland (1971), Garland *et al.* (1973) and Roach *et al.* (1976) are shown. The extinction and liquid water contents calculated from the 26 measured size distributions are divided according to radiation (circles) or advection (squares) fog. We see from the figure that radiation fogs are generally more effective scatterers than advection fogs with the same liquid water content because they contain more droplets in the Mie resonance region that contribute a significant part of the extinction but contribute only a marginal amount to the liquid water content.

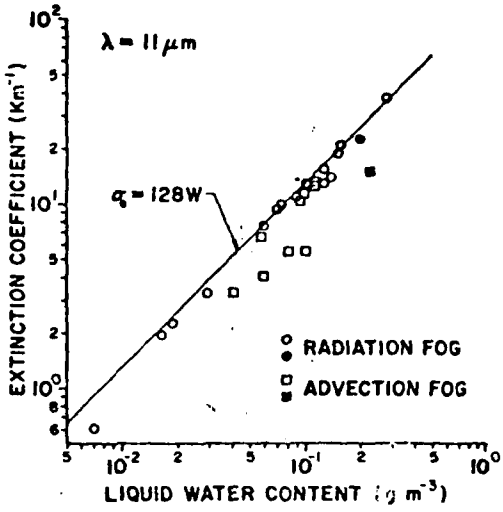

FIG. 3. As in Fig. 2 except for λ = 11 μm. The predicted relation between extinction and liquid water content given by Eq. (1) is shown by the straight line. Because the $Q_e = cx$ approximation is generally better satisfied for radiation fogs, those points fall closer to the straight line prediction.

At λ = 11 μm (Fig. 3), although the $Q_e = cx$ approximation is within a factor of about 2 for both radiation and advection fog results, the approximation is generally in better agreement with the radiation fog results. The explanation is that the $Q_e = cx$ approximation is only strictly valid providing fog droplets have $r \leq 14$ μm (Chýlek, 1978) and radiation fogs better satisfy this condition than do advection fogs. The degree to which this maximum radius condition is violated can be determined for two fog examples from Fig. 5. Shown is the differential extinction coefficient at λ = 11 μm for a radiation fog (Fig. 3, solid circle) and an advection fog (Fig. 3,

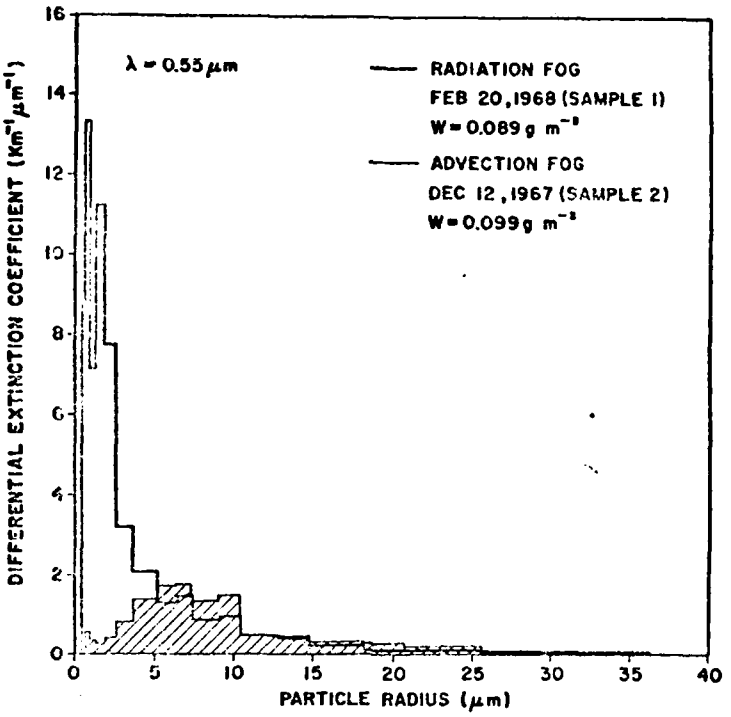

FIG. 4. Differential extinction coefficients at $\lambda = 0.55$ μm versus droplet radius for a radiation fog (solid circle in Fig. 2) and an advection fog (solid square in Fig. 2) with about the same liquid water content. The areas under the curves are a measure of the total extinction coefficients (35 km^{-1} for the radiation fog versus 15.8 km^{-1} for the advection fog). For the radiation fog, 69% of the extinction is contributed by droplets having $r \leq 3$ μm, compared to only 6% for the advection fog.

solid square) again having about the same liquid water content. For the radiation fog 69% of the extinction arises from droplets with radii less than the maximum value r_m = 14 μm, while for the advection fog this value drops to 33%. A survey of all the differential extinction coefficient versus particle radius graphs similar to those shown in Fig. 5 for the radiation fogs of Garland (1971), Garland *et al.* (1973) and Roach *et al.* (1976) in Fig. 3 show that in all cases extinction at $\lambda = 11$ μm is dominated by droplets with $r \leq 14$ μm. On the other hand, a survey of the differential extinction coefficient graphs for the advection fogs presented in Fig. 3, and also the advection fog of Fumai (1973), show that for about one-half of the distributions, extinction at $\lambda = 11$ μm is dominated by droplets with $r > 14$ μm. Since the absorption efficiency factor for these larger particles is estimated by the $Q_a = cx$ approximation (see Chýlek, 1978), the numerical calculation of the extinction for these advection fogs fall below the $Q_a = cx$ prediction in Fig. 3. For the remaining half of the advection fogs, droplets with $r > 14$ μm dominate extinction and the points fall within 20% of the $Q_a = cx$ prediction. Thus, while droplets with $r \leq 14$ μm dominate extinction at $\lambda = 11$ μm for radiation fog, this is not always the case for advection fog, where the presence of larger droplets partially destroys the size distribution independent linear relation (1).

4. $Q_a = c'x$ approximation for absorption

Realizing that the $Q_e = cx$ approximation works reasonably well for fog at $\lambda = 11$ μm, and for haze at shorter wavelengths, we checked to see if a similar approximation for fog droplet absorption might hold in the $\lambda = 3$–5 μm and $\lambda = 8$–12 μm atmospheric window spectral regions.

The absorption coefficient σ_a for a polydispersion of droplets described by the size distribution $n(r)$ is given by

$$\sigma_a = \int \pi r^2 Q_a(m, x) n(r) dr, \qquad (5)$$

where $Q_a(m, x)$ is the Mie efficiency factor for absorption for a water droplet with refractive index $m(\lambda)$ and size parameter $x = 2\pi r/\lambda$. Plots of the efficiency factor for absorption Q_a vs x for $\lambda = 3.8$,

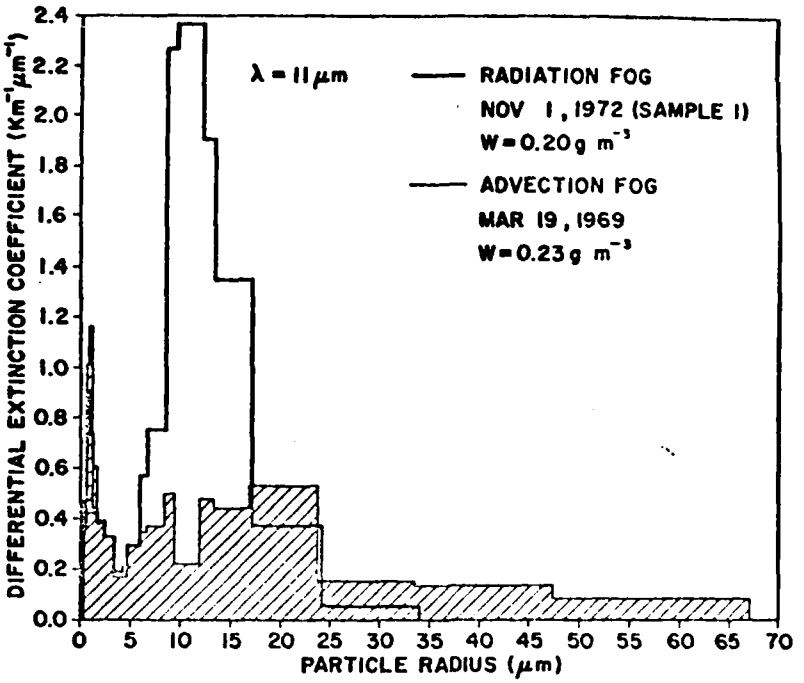

FIG. 5. Differential extinction coefficients at $\lambda = 11$ μm versus droplet radius for a radiation fog (solid circle in Fig. 3) and an advection fog (solid square in Fig. 3) with about the same liquid water content. The total extinction for the radiation fog is 22.6 km^{-1} compared to 15.0 km^{-1} for the advection fog. The fraction of extinction contributed by droplets with $r \leq 14$ μm (the maximum value allowed in the $Q_e = cx$ approximation) is 69% for the radiation fog, decreasing to 33% for the advection fog. Thus the prediction between extinction (at $\lambda = 11$ μm) and liquid water content [given by Eq. (1) and shown in Fig. 3] is a better approximation for radiation fogs than for advection fogs.

9.5 μm are shown in Figs. 6 and 7. Again we find, as Chýlek (1978) found for extinction, that Q_a can be well approximated by $Q_a(x,\lambda) \approx c'(\lambda)x$, providing $x \leq x_m$.

Using this linear approximation for Q_a in (5) gives

$$\sigma_a = \frac{3\pi c'}{2\lambda\rho} \int \frac{4\pi r^3}{3} n(r)dr. \qquad (6)$$

Thus, explicit dependence on the size distribution disappears and leads to the absorption coefficient being linearly related to liquid water content W according to

$$\sigma_a = \frac{3\pi c'}{2\lambda\rho} W. \qquad (7)$$

As in the case of extinction the restriction that $x \leq x_m$ need not be strictly satisfied, but water droplets with radii greater than the value $r_m = \lambda x_m/2\pi$ must not contribute excessively to either absorption or liquid water content. Numerical values of the maximum radii r_m at various wavelengths λ as well as the slope c' of a straight line approximating Q_a for $x = x_m$, are given in Table 1.

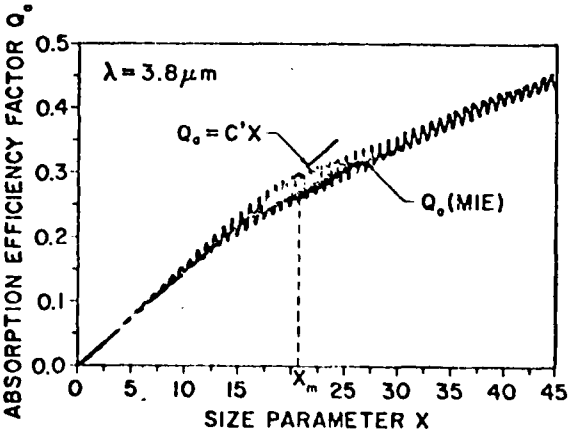

FIG. 6. The efficiency factor for absorption Q_a for water versus droplet size parameter x at a wavelength $\lambda = 3.8$ μm (index of refraction $m = 1.364 - 0.0034i$). The efficiency factor can be approximated by a straight line $Q_a = c'x$ providing $x \leq x_m$. The approximation overestimates the exact value of Q_a for some size parameters, but underestimates it for others. These two errors tend to cancel leading to the absorption coefficient being linearly related to liquid water content according to equation (7).

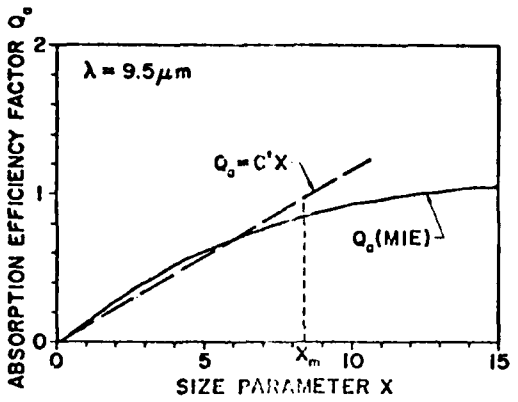

FIG. 7. As in Fig. 6 except for $\lambda = 9.5\ \mu m$ (index of refraction of water $m = 1.243-0.0443i$). The efficiency factor for absorption can again be approximated by a straight line $Q_a = c'x$ providing $x \leq x_m$.

Also given are values of the quantity $3\pi c'/2\lambda\rho$ which if multiplied by the liquid water content give the absorption coefficient. In order that these predicted relationships (and maximum radius conditions) between droplet absorption and liquid water content may be compared to the corresponding results for extinction, the values of x_m, r_m, etc., for the $Q_e = cx$ approximation (Chýlek, 1978) for extinction also appear in Table 1. The values of x_m, r_m and c for extinction are sometimes slightly different from those of Chýlek (1978) since there is some leeway in the subjective procedure for approximating the efficiency factor $Q_e(x)$ by a linear function of size parameter x. We see from the table that the limiting radius r_m depends strongly on wavelength and is in general markedly different for absorption and extinction at a particular wavelength. An exception is at $\lambda = 9.5\ \mu m$, where the limiting radii are $r_m = 13\ \mu m$ for absorption as compared to $r_m = 12.5\ \mu m$ for extinction. Thus for fog droplet distributions that have radii $r \leq 12.5\ \mu m$ (i.e., most radiation fogs) we can predict from Table 1 that absorption contributes 29% of the extinction at $\lambda = 9.5\ \mu m$, independent of the form of the droplet size distribution. However, there is obviously no unique relation between fog absorption and extinction for all wavelengths.

Since we have verified the $Q_e = cx$ approximation for extinction at $\lambda = 11\ \mu m$, which requires that droplets have maximum radius $r_m = 14\ \mu m$, is adequate for atmospheric fogs, we suspect the $Q_a = c'x$ approximation for absorption is adequate for fog at selected wavelengths also having $r_m = 14\ \mu m$. From Table 1 we see that wavelengths $\lambda = 3.8$, 4, 5.3 and 9.5 μm either satisfy or nearly satisfy this criterion. Therefore, we might expect a linear relation between fog absorption and fog liquid water content according to (7), independent of the droplet size distribution, for these particular wavelengths.

To check this contention we have calculated the volume absorption coefficient $\sigma_a(\lambda)$ using a Mie scattering program according to Eq. (5) for the previously mentioned 341 fog and haze size distributions at several different wavelengths. As in the extinction calculations we have assumed particle refractive indexes of water, and have thus neglected refractive index differences that might be caused by the presence of contaminants such as sea salt and ammonium sulfate. The results at $\lambda = 3.8$, 9.5 μm plotted as a function of fog liquid water content together with the $Q_a = c'x$ approximation (7) are shown in Figs. 8 and 9. We see that although the numerical results are slightly better approximated at $\lambda = 3.8\ \mu m$ as compared to $\lambda = 9.5\ \mu m$, at both wavelengths the linear relation (7) is within a factor 2.5 of the numerical results for all 341 fog and haze size distributions. Examination of results at numerous other infrared wavelengths show that even though the maximum radius condition is sometimes violated, for $\lambda = 3.5$–$5.3\ \mu m$, 8–10 μm all numerical results for the 341 fog distributions are within a factor 2.5 of the predictions between absorption and liquid water content given by relation (7) and listed in Table 1, and in most cases the agreement is within a factor 2. However, at wavelengths $\lambda = 10.5$–$12\ \mu m$, the numerical results differ by as much as a factor 4 from the linear relation (7).

Previously, Platt (1976) found an approximate linear relation between the absorption coefficient

TABLE 1. At a given wavelength λ the efficiency factor for absorption Q_a (and extinction Q_e) can be approximated by a straight line $Q_a = c'x$ ($Q_e = cx$) for size parameters $x \leq x_m$. The values of x_m and c' (and c) are determined from the efficiency curves (see, e.g., Figs. 6 and 7). If we know the maximum radius r_m of droplets in a given size distribution, the table gives the wavelength λ at which a linear relationship between absorption (or extinction) and liquid water content exists, and the appropriate value of the parameter c' (or c). The value of the quantity $3\pi c'/2\lambda\rho$ (or $3\pi c/2\lambda\rho$) multiplied by the liquid water content W gives the absorption coefficient σ_a (or extinction coefficient σ_e).

	Absorption				Extinction			
λ (μm)	x_m	r_m (μm)	c'	$3m''/2\lambda\rho$ (cm^2 g^{-1})	x_m	r_m (μm)	c	$3\pi c/2\lambda\rho$ (cm^2 g^{-1})
3.0	2.5	1.1	0.58	9.1×10^3	3.2	1.5	0.85	13.3×10^3
3.5	14	8.0	0.047	0.50×10^3	5.9	3.3	0.72	9.6×10^3
3.8	21	13	0.015	0.18×10^3	6.5	4.0	0.66	8.2×10^3
4.0	22	14	0.018	0.22×10^3	6.7	4.3	0.64	7.6×10^3
4.5	14	10	0.047	0.49×10^3	7.0	5.0	0.59	6.1×10^3
5.0	14	11	0.044	0.41×10^3	7.2	5.8	0.56	5.3×10^3
5.3	16	14	0.035	0.31×10^3	7.5	6.3	0.56	5.0×10^3
8.0	7.6	9.7	0.10	0.61×10^3	7.3	9.3	0.51	3.0×10^3
8.5	8.2	11	0.11	0.69×10^3	7.9	10.7	0.45	2.5×10^3
9.0	8.0	12	0.11	0.52×10^3	8.0	11.5	0.44	2×10^3
9.5	8.4	13	0.12	0.58×10^3	8.2	12.5	0.41	2.0×10^3
10.0	7.0	11	0.13	0.63×10^3	8.8	13	0.38	1.8×10^3
10.5	6.0	11	0.16	0.70×10^3	8.6	14	0.33	1.5×10^3
11.0	4.1	7.2	0.21	0.93×10^3	8.1	14	0.31	1.3×10^3
11.5	3.1	5.7	0.30	1.25×10^3	8.0	9.1	0.47	1.9×10^3
12.0	2.3	4.5	0.42	1.65×10^3	4.9	9.3	0.44	1.7×10^3
12.5	1.8	3.7	0.58	2.2×10^3	3.7	7.3	0.58	2.2×10^3

σ_a at $\lambda = 11$ μm and liquid water content W of non-precipitating stratocumulus clouds. Platt performed Mie calculations on 25 measured cloud droplet distributions, plotted the values of σ_a at $\lambda = 11$ μm vs W, did a least-squares fit through the resulting data points and obtained $\sigma_a = 76.5\ W$, comparing modestly well with our Eq. (7) prediction from Table 1 of $\sigma_a = 93\ W$, where the absorption is in km^{-1} and the liquid water content in g m^{-3}. The reason for our overprediction of the absorption is that a significant number of droplets in Platt's distributions have radii >7.2 μm, the maximum value allowable in the $Q_a = c'x$ approximation at $\lambda = 11$ μm. Had Platt chosen a slightly shorter wavelength, say, $\lambda = 9.5$ μm, he would have found an even better correlation of absorption and liquid water content, as well as better agreement with our linear prediction (7), since the maximum radius restriction is more nearly satisfied for clouds at the shorter wavelength.

5. Application of extinction—absorption-liquid water content relationships

The unique, linear, size-distribution-independent relationship between extinction at $\lambda \approx 11$ μm and liquid water content, and between absorption at $\lambda \approx 3.8$, 9.5 μm and liquid water content in fog has several practical applications. For example, for a fog with liquid water content $W = 0.1$ g m^{-3} we predict extinction and absorption coefficients of $\sigma_e(\lambda = 11\ \mu\text{m}) = 13$ km^{-1}, $\sigma_a(3.8\ \mu\text{m}) = 1.8$ km^{-1}, $\sigma_a(5.3\ \mu\text{m}) = 3.1$ km^{-1} and $\sigma_a(9.5\ \mu\text{m}) = 5.7$ km^{-1}. Integrated liquid water content along a path in fog and haze could be inferred from a CO_2 laser ($\lambda = 10.6$ μm) transmissometer measurement according to (1). Of course the path must be short enough that multiple-scattering effects and forward-scattering corrections (Deepak and Box, 1978) are negligible. Carlon *et al.* (1977) previously realized this application for a transmission measurement at $\lambda = 12.5$ μm. An application of the σ_a–W relationship is that liquid water content of fog at a particular point could be determined by measurement of fog droplet absorption in the spectral region $\lambda \approx 3.8$, 9.5 μm according to Eq. (7). The spectrophone technique has been demonstrated to be suitable for *in situ* measurement of particulate absorption by Bruce and Pinnick (1977), so that measurement of fog droplet absorption with either a CO_2 laser spectrophone tuned to a wavelength $\lambda \approx 9.5$ μm, or a DF laser spectrophone ($\lambda \approx 3.8$ μm) could be used to infer fog liquid water content. Of course the spectrophone measurement of absorption could also be used to infer fog extinction at $\lambda \approx 11$ μm. The Eq. (7) relation between fog absorption and liquid water content might also be used in calculation of fog emissivities.

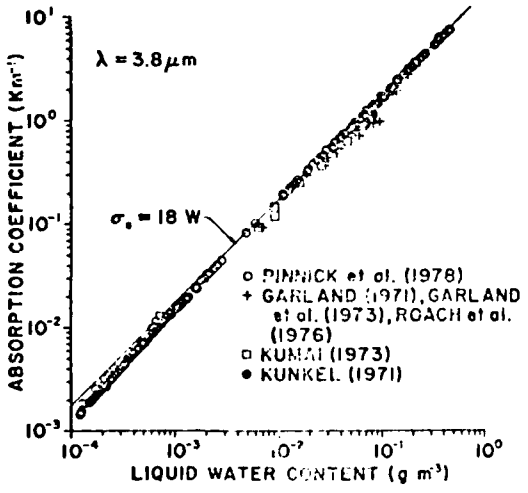

FIG. 8. Variation of absorption coefficient with liquid water content in atmospheric fog and haze for 341 size distribution measurements made at different geographic locales and under a variety of meteorological conditions. In the infrared region around $\lambda = 3.8$ μm there exists a linear, size-distribution-independent relation between the volume absorption coefficient σ_a and the liquid water content W of the form of Eq. (7). Consequently, the results of all measurements are close to a straight line. The predicted relation between absorption σ_a and liquid water content W according to Eq. (7) is shown by the straight line.

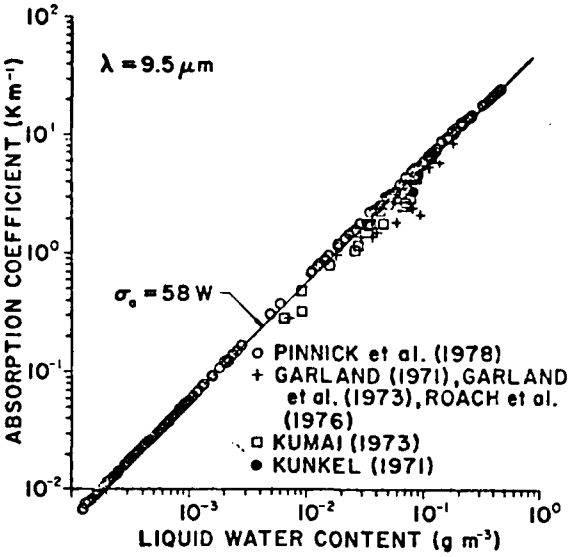

FIG. 9. As in Fig. 8 except for $\lambda = 9.5$ μm.

6. Conclusions

Chýlek's (1978) prediction of a linear relation, independent of the form of the size distribution, between extinction at $\lambda = 11$ μm and liquid water content of fog has been verified within a factor 2 for 341 different fog and haze droplet distribution

measured under a variety of meteorological conditions. The prediction generally works better for radiation fogs than advection fogs. A similar linear relation between fog droplet absorption at $\lambda \approx 3.8$, 9.5 μm and liquid water content has been derived and validated using the same 341 distributions. However, there exists no size-distribution-independent relation between extinction in the visible ($\lambda = 0.55$ μm) and fog liquid water content. Three practical applications of these findings are suggested: 1) inference of fog-integrated liquid water content along a path by measurement of laser transmission (at $\lambda \approx 11$ μm) along that path; 2) inference of fog liquid water content at a particular point from measurement of fog droplet absorption with a DF or CO_2 laser spectrophone; and 3) calculation of fog emissivities in the infrared from knowledge of fog liquid water content.

Acknowledgment. We gratefully acknowledge John A. Garland, Environmental and Medical Sciences Division, Harwell, who supplied his raw data of fog size distributions. One of us (P.C.) was partially supported by a grant from the U.S. Army Research Office. On request the authors will send to interested researchers a more detailed report of this work.

REFERENCES

Arnulf, A., J. Bricard, E. Curé and C. Véret, 1957: Transmission by haze and fog in the spectral region 0.35 to 10 microns. *J. Opt. Soc. Amer.*, 47, 491–498.

Bruce, C. W., and R. G. Pinnick, 1977: In situ measurements of aerosol absorption with a resonant CW laser spectrophone. *Appl. Opt.*, 16, 1762–1765.

Carlon, H. R., D. Anderson, M. Milham, T. Tarnove and R. Frickel, 1977: Infrared extinction spectra of some common liquid aerosols. *Appl. Opt.*, 16, 1598–1605.

Chýlek, Petr, 1978: Extinction and liquid water content of fogs. *J. Atmos. Sci.*, 35, 296–300.

Deepak, Adarsh, and M. A. Box, 1978: Forward scattering corrections for optical extinction measurements in aerosol media. 2: Polydispersions. *Appl. Opt.*, 17, 3169–3176.

Eldridge, R. G., 1961: A few fog drop-size distributions. *J. Appl. Meteor.*, 18, 671–676.

——, 1966: Haze and fog aerosol distributions. *J. Atmos. Sci.*, 23, 605–613.

——, 1971: The relationship between visibility and liquid water content in fog. *J. Atmos. Sci.*, 28, 1183–1186.

Garland, J. A., 1971: Some fog droplet size distributions obtained by an impaction method. *Quart. J. Roy. Meteor. Soc.*, 97, 483–494.

——, J. R. Branson and L. C. Cox, 1973: A study of the contribution of pollution to visibility in a radiation fog. *Atmos. Environ.*, 7, 1079–1092.

Hale, G. M., and M. R. Querry, 1973: Optical constants of water in the 200 nm to 20 μm wavelength region. *Appl. Opt.*, 12, 555–563.

Hänel, G., 1976: The properties of atmospheric aerosol particles as functions of relative humidity at thermodynamic equilibrium with the surrounding moist air. *Advances in Geophysics*, Vol. 19, Academic Press, 73–188.

——, and K. Bullrich, 1978: Physico—chemical property models of tropospheric aerosol particles. *Beitr. Phys. Atmos.*, 51, 129–138.

Kumai, Motoi, 1973: Arctic fog droplet size distribution and its effect on light attenuation. *J. Atmos. Sci.*, 30, 635–643.

Kunkel, B. A., 197 Fog drop-size distributions measured with a laser hologram camera. *J. Appl. Meteor.*, 10, 482–486.

May, K. R., 1945: The cascade impactor: An instrument for sampling aerosols. *J. Sci. Instrum.*, 22, 187–195.

——, 1961: Fog droplet sampling using a modified impactor technique. *Quart. J. Roy. Meteor. Soc.*, 87, 535–548.

Pinnick, R. G., D. L. Hoihjelle, G. Fernandez, E. B. Stenmark, J. D. Lindberg, S. G. Jennings and G. B. Hoidale, 1978: Vertical structure in atmospheric fog and haze and its effects on IR and visible extinction. *J. Atmos. Sci.*, 35, 2020–2032.

Pilié, R. J., E. J. Mack, K. C. Kocmond, W. J. Eadie and C. W. Rogers, 1975: The life cycle of valley fog. Part II: Fog microphysics. *J. Appl. Meteor.*, 14, 364–374.

Platt, C. M. R., 1976: Infrared absorption and liquid water content in stratocumulus clouds. *Quart. J. Roy. Meteor. Soc.*, 102, 553–561.

Roach, W. T., R. Brown, S. J. Caughey, J. A. Garland and C. J. Readings, 1976: The physics of radiation fog: I—a field study. *Quart. J. Roy. Meteor. Soc.*, 102, 313–333.

APPENDIX 3

PERTURBATION APPROACH TO LIGHT SCATTERING BY NON-SPHERICAL PARTICLES

J. T. Kiehl
State Univ. of N.Y. at Albany, Department of Atmospheric Science, Albany, NY 12222, and National Center for Atmospheric Research, Boulder, CO 80307

M. W. Ko
Atmospheric and Environmental Research, Cambridge, MA 12138

A. Mugnai
CNR-LPS, Elettrofisica Atmosferica, Frascati, Italy

Petr Chýlek
State Univ. of N.Y. at Albany, Atmospheric Sciences Research Center, Albany, NY 12222, and National Center for Atmospheric Research, Boulder, CO 80307

ABSTRACT

Applying perturbation theory we have derived the first order perturbation corrections to the scattering characteristics for the case of light scattering by slightly deformed spheres. Numerical results are compared with those obtained using the extended boundary condition method. The range of applicability of the first order perturbation corrections are discussed.

The application of perturbation theory to light scattering by non-spherical particles has experienced very little development since it was first derived by Yeh (1964, 1965) and Erma (1968). It is the purpose of this report to investigate the application of first order perturbation theory to light scattering by various non-spherical particles. The results of perturbation theory are then compared with calculations for the same particles using the extended boundary condition method (EBCM) developed by Waterman (1971), and Barber and Yeh (1975).

A general formalism for calculating the n^{th} order perturbation term has been developed by Yeh (1964, 1965) and Erma (1968). The particle is assumed to be of the form:

$$r = r_s \left(1 + \varepsilon f(\theta,\phi)\right) \tag{1}$$

where r_s is the radius of an unperturbed sphere, $f(\theta,\phi)$ describes the shape of the irregularity on the sphere. It is further assumed that $\varepsilon << 1$ and that $|\varepsilon f(\theta,\phi)| < 1$. The calculations reported herein used the following functional forms for $f(\theta,\phi)$:

$$f(\theta,\phi) = T_2(\cos\theta) \tag{2}$$

$$f(\theta,\phi) = T_4(\cos\theta) \tag{3}$$

where $T_n(\cos\theta)$ is the n^{th} order Chebyshev polynomial.

The shapes of these particles are illustrated in Figure 1. The particle is assumed to be oriented such that it is rotationally symmetric about the z-axis. The incident light is assumed to be traveling in the z-direction with E vector in the x-direction. First order perturbation theory assumes that the scattering coefficients for the non-spherical particle can be expressed as

$$a_n = a_n^0 + \varepsilon\, a_n^1 , \tag{4}$$

$$b_n = b_n^0 + \varepsilon\, b_n^1 . \tag{5}$$

where a_n^0, b_n^0 are the Mie scattering coefficients for a sphere of radius r_s; a_n^1, b_n^1 are the first order corrections due to the non-sphericity of the particle.

Calculations were performed for the case where the index of refraction $m = 1.5$ and $\varepsilon = \pm 0.1$. Results for other indexes of refraction and values of ε have been reported in Chýlek *et al.* (1978). The efficiencies are calculated by normalizing the extinction cross sections by πr_s^2.

Figure 2 shows the extinction efficiency for both perturbation theory and EBCM for the case of $f(\theta,\phi) = T_2(\theta)$ and $\varepsilon = +0.1$. The extinction efficiency for a sphere of radius r_s is also shown in Figure 2. It is evident from Figure 2 that perturbation theory agrees quite well with EBCM for $x_s < 6$. For values of $x_s > 6$ there

FIG. 1. The two shapes considered are: a) $r = r_s\left(1 \pm \varepsilon\, T_2(\cos\theta)\right)$, b) $r = r_s\left(1 \pm \varepsilon\, T_4(\cos\theta)\right)$.

FIG. 2. The extinction efficiency for light scattering by a particle whose shape is given by $r = r_s\left(1 + 0.1\, T_2(\cos\theta)\right)$. The solid line (——) is for a sphere with $r = r_s$. The dashed line (---) represents the exact results of the EBCM. The dotted line (···) represents the results of first order perturbation theory.

is very poor agreement between perturbation theory and EBCM due to the narrowness of the resonance in the extinction efficiency. The effect of the width of a resonance on perturbation theory has been discussed by Chýlek *et al.* (1978). There it was shown that in the resonance region one would expect perturbation theory to apply when

$$|\varepsilon| < \Gamma/2\, x_s \,, \qquad (6)$$

where Γ is the half width of a Lorentzian shaped resonance. Equation (6) implies that for large values of x_s, where Γ is expected to be small, one would need a very small ε for perturbation theory to agree with the exact calculations.

Figure 3 shows the extinction efficiency for the same shape function but with $\varepsilon = -0.1$. The observations made above for Figure 2 apply to this case.

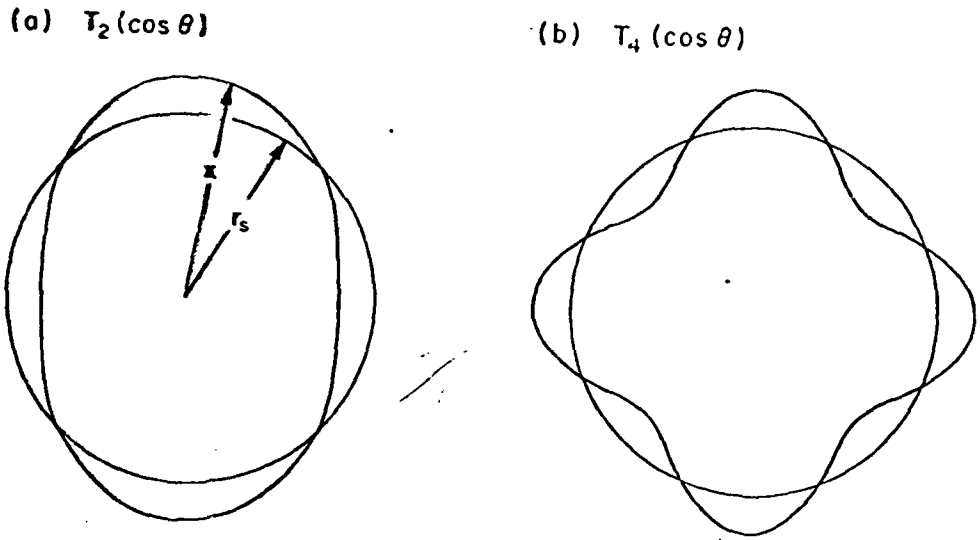
(a) $T_2(\cos\theta)$
(b) $T_4(\cos\theta)$
x
r_s

fig 1

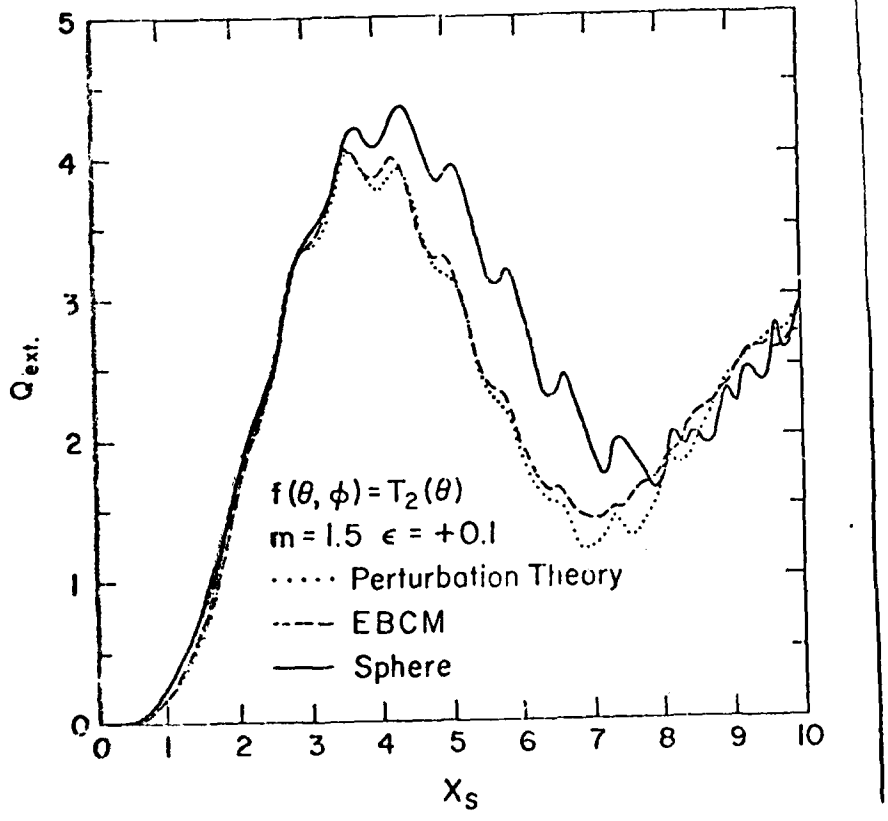
$Q_{ext.}$
X_s
$f(\theta, \phi) = T_2(\theta)$
m = 1.5 ϵ = +0.1
Perturbation Theory
EBCM
Sphere
0
1
2
3
4
5
6
7
8
9
10

fig 2

The difference between perturbation theory and EBCM can best be illustrated by considering the relative difference between the results obtained using these two methods. This difference is defined as

$$\delta = \frac{Q_{ext}^{Pert} - Q_{ext}^{EBCM}}{Q_{ext}^{EBCM}} \tag{7}$$

which is a function of x_s. Figure 4 shows the absolute value of equation (7) for the case of $\varepsilon = +0.1$ and $f(\theta,\phi) = T_2(\theta)$. Since terms of order ε^2 have been neglected in these calculations an error of 10^{-2} would be expected. It can be seen from Figure 4 that the difference lies between 10^{-3} and 10^{-1}. A striking feature of this

FIG. 3. The extinction efficiency for light scattering by a particle whose shape is given by $r = r_s\left(1 - 0.1\ T_2(\cos\theta)\right)$. The solid line (——) is for a sphere of radius $r = r_s$. The dashed line (---) represents the exact results of the EBCM. The dotted line (···) represents the results of first order perturbation theory.

FIG. 4. The absolute value of the relative difference between perturbation theory and the EBCM for the particle: $r = r_s\left(1 + 0.1\ T_2(\cos\theta)\right)$ as a function of $x_s = 2\pi r_s/\lambda$.

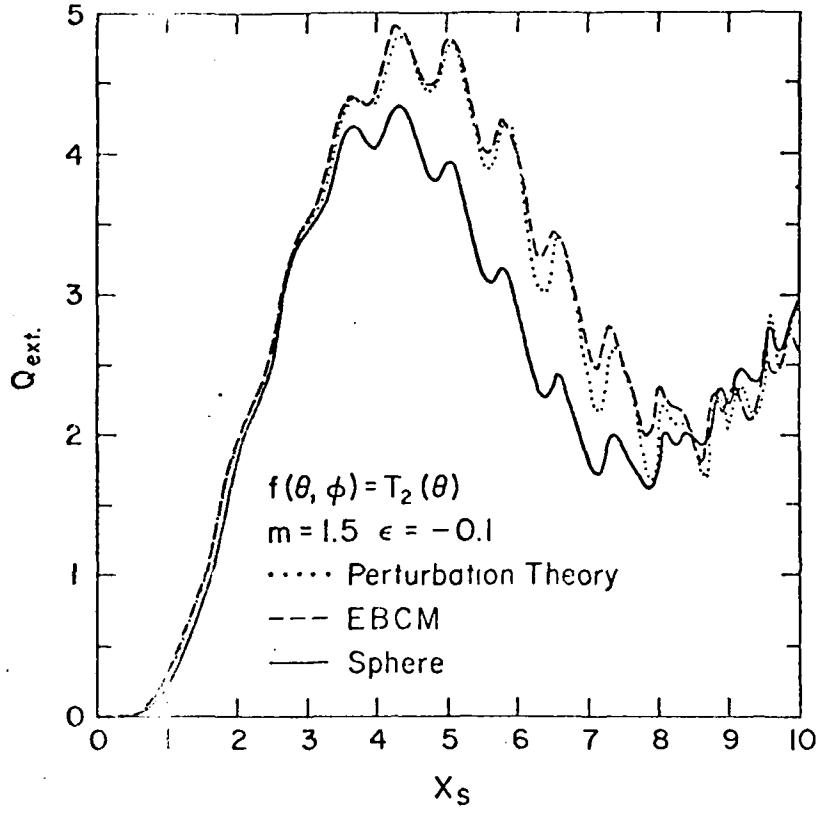
$Q_{ext.}$
X_S
$f(\theta, \phi) = T_2(\theta)$
$m = 1.5 \quad \epsilon = -0.1$
····· Perturbation Theory
--- EBCM
—— Sphere
0
1
2
3
4
5
6
7
8
9
10

fig 3

Kiehl

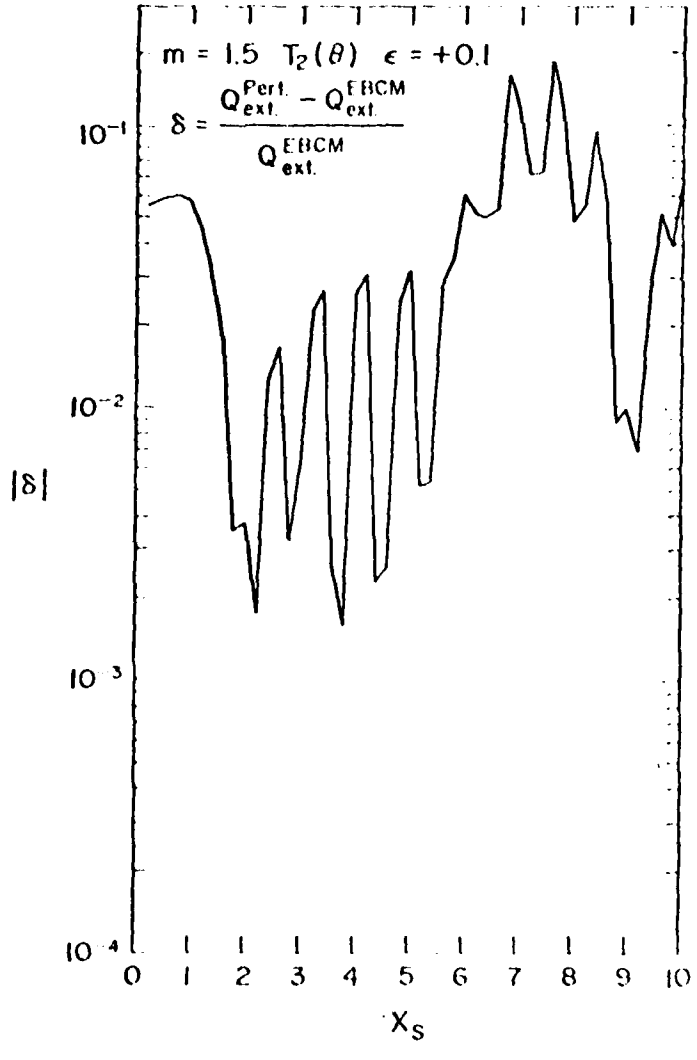
m = 1.5 $T_2(\theta)$ $\epsilon = +0.1$
$\delta = \frac{Q_{ext.}^{Pert.} - Q_{ext.}^{EBCM}}{Q_{ext.}^{EBCM}}$
10^{-1}
10^{-2}
10^{-3}
10^{-4}
$|\delta|$
0 1 2 3 4 5 6 7 8 9 10
X_S

Fig 4

Kiehl

figure is the oscillatory behavior of $|\varepsilon|$. These oscillations are due to the resonance effect discussed above for Figures 2 and 3. There exists a one-to-one correspondence between the position of the maxima in relative difference in Figure 4 and the position of the resonance of the extinction curve. An overall growth in absolute relative difference can be observed for increasing values of x_s due to the narrowing of the resonances.

Similar calculations for $f(\theta,\phi) = T_4(\theta)$ and $\varepsilon = +0.1$ are shown in Figure 5. For this case little difference can be seen to exist for $x_s < 7$. It is also observed that the $T_4(\theta)$ particle has a smaller extinction than the sphere for this size range. Figure 6 illustrates the extinction efficiency for a shape function $f(\theta,\phi) = T_4(\theta)$ and $\varepsilon = -0.1$.

Figure 7 shows the absolute value of the relative difference for the $T_4(\theta)$ particle with $\varepsilon = +0.1$ as a function of x_s. The relative difference from this figure lies between 2.5×10^{-4} to 2.2×10^{-1}. The oscillatory behavior of this difference correlates with the resonances in Figure 5.

FIG. 5. The extinction efficiency for light scattering by a particle whose shape is given by $r = r_s\left(1 + 0.1\ T_4(\cos\theta)\right)$. The solid line (——) is for a sphere of radius $r = r_s$. The dashed line (---) represents the exact results of the EBCM. The dotted line (···) represents the results of first order perturbation theory.

FIG. 6. The extinction efficiency for light scattering by a particle whose shape is given by $r = r_s$ $(1 - 0.1\ T_4(\cos\theta)$. The solid line (——) is for a sphere of radius $r = r_s$. The dashed line (---) represents the exact results of the EBCM. The dotted line (···) represents the results of first order perturbation theory

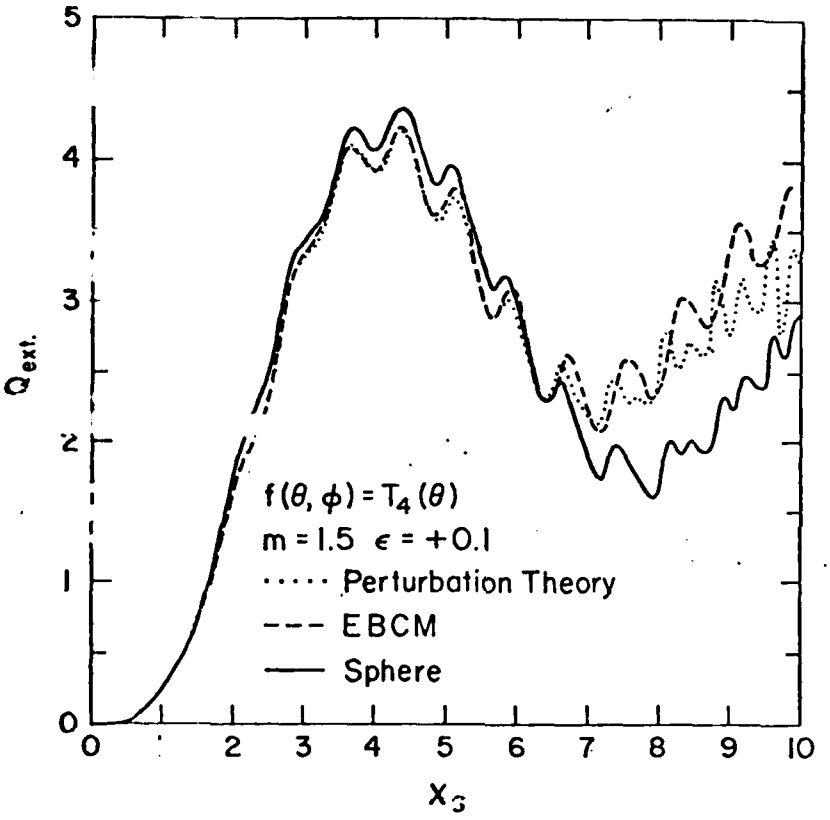
5
4
3
2
1
0
$Q_{ext.}$
0
2
3
4
5
6
7
8
9
10
X_3
$f(\theta, \phi) = T_4(\theta)$
$m = 1.5 \quad \epsilon = +0.1$
····· Perturbation Theory
--- EBCM
—— Sphere

fig 5

Kiehl

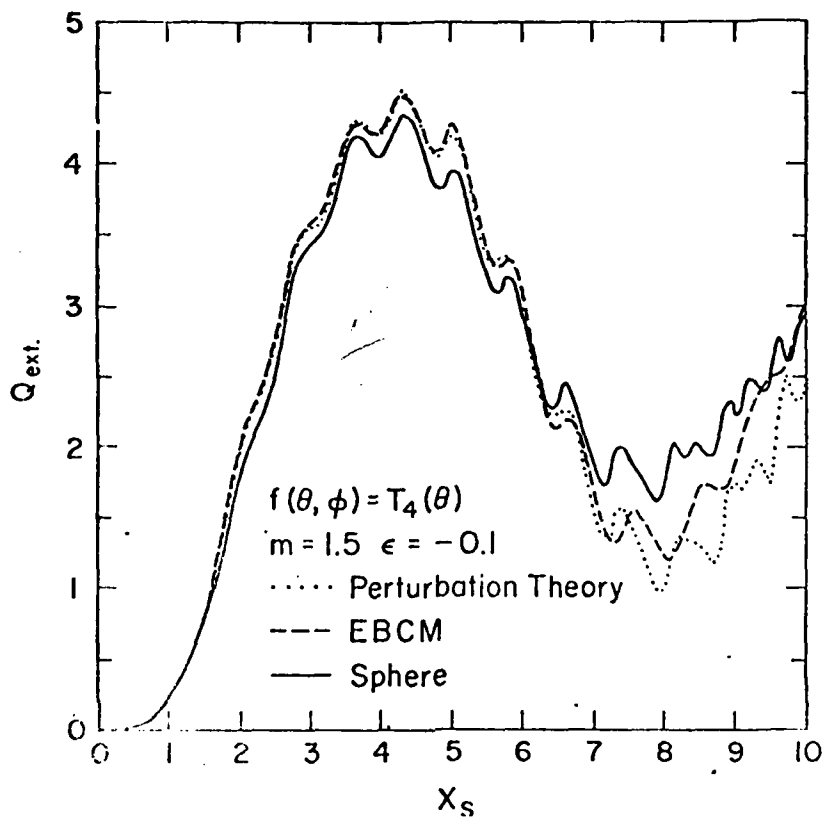
5
4
3
2
1
0
$Q_{ext.}$
0 1 2 3 4 5 6 7 8 9 10
X_s
$f(\theta, \phi) = T_4(\theta)$
$m = 1.5 \quad \epsilon = -0.1$
····· Perturbation Theory
--- EBCM
—— Sphere

fig 6

Kiehl

In conclusion, this study indicates that first order perturbation theory as applied to light scattering by non-spherical particles is limited to small deformations and low values of the size parameter. The limitation arises because of the breakdown of first order perturbation theory in the region of resonances of the scattering coefficients. However, these problems can be eliminated by taking higher order terms in the perturbation expansion. The computational feasibility of such calculations is possible since these calculations require little storage and computer time.

FIG. 7. The absolute value of the relative difference between perturbation theory and the EBCM for the particle: $r = r_s\{1 + 0.1 T_4(\cos\theta)\}$ as a function of $x_s = 2\pi r_s/\lambda$.

Acknowledgement. This work was supported in part by the U.S. Army Research Office. The National Center for Atmospheric Research is sponsored by the National Science Foundation.

REFERENCES

Barber, P. and Yeh, C., 1975, *Appl. Opt.*, *14*, 2864.
Chýlek, P., Kiehl, J. T., Ko, M. W., 1978, Third Conference on Atmospheric Radiation, American Meteorological Society, 1978.
Erma, V., 1968, *Phys. Rev.*, *179*, 1238.
Waterman, P. C., 1971, *Phys. Rev. D*, *3*, 825.
Yeh, C., 1964, *Phys. Rev.*, *135*, A1193.
Yeh, C., 1965, *J. Math. Phys.*, *6*, 2008.

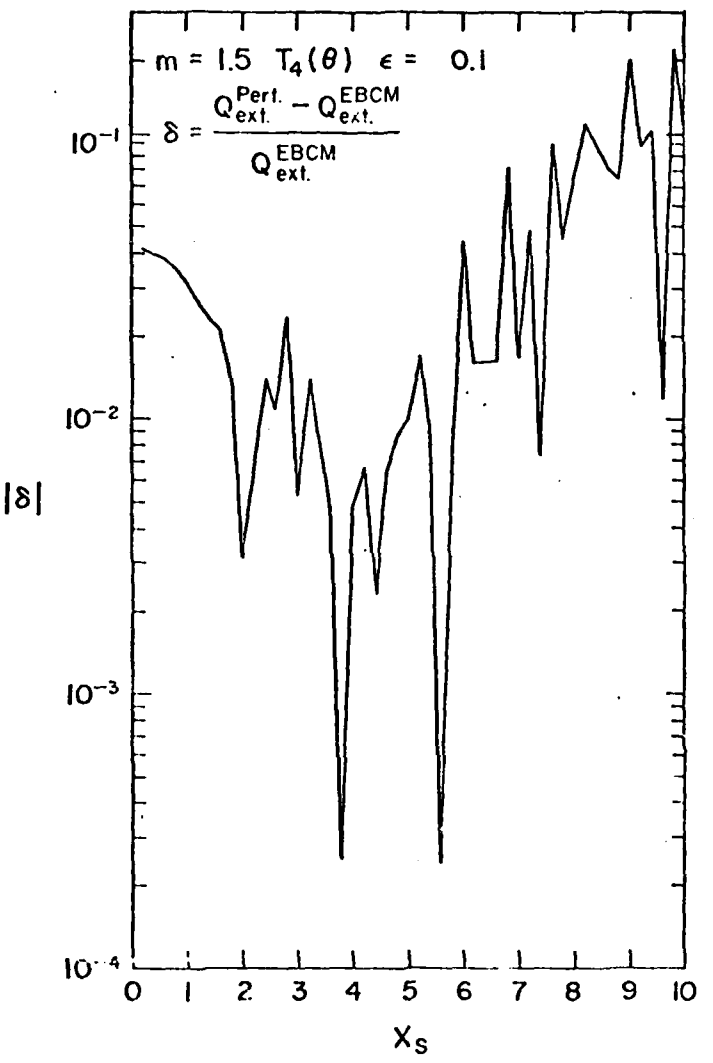
m = 1.5 $T_4(\theta)$ ϵ = 0.1
$\delta = \frac{Q_{ext.}^{Pert.} - Q_{ext.}^{EBCM}}{Q_{ext.}^{EBCM}}$
10^{-1}
10^{-2}
10^{-3}
10^{-4}
$|\delta|$
0 1 2 3 4 5 6 7 8 9 10
X_S

Fig. 7

Kieh!

APPENDIX 4

SURFACE WAVES IN LIGHT SCATTERING BY SPHERICAL AND NON-SPHERICAL PARTICLES

Petr Chýlek
State Univ. of N.Y. at Albany, Atmospheric Sciences Research Center, Albany, NY 12222, and National Center for Atmospheric Research, Boulder, CO 80307

J. T. Kiehl
State Univ. of N.Y. at Albany, Department of Atmospheric Science, Albany, NY 12222, and National Center for Atmospheric Research, Boulder, CO 80307

M. K. W. Ko
Atmospheric and Environmental Research, Cambridge, MA 02138

A. Ashkin
Bell Telephone Laboratories, Holmdel, NJ 07733

ABSTRACT

Resonances in partial wave scattering amplitudes a_n and b_n are responsible for the ripple structure of the extinction curve and for sharp peaks in the backscattering (glory). A connection between the resonances and surface waves is suggested.

1. RESONANCES IN PARTIAL WAVE AMPLITUDES a_n AND b_n

It is convenient to write the Mie partial wave amplitudes a_n and b_n in the form

$$a_n = \frac{A_n}{A_n - iC_n} \quad (1a) \; ; \quad b_n = \frac{B_n}{B_n - iD_n} \quad (1b)$$

where A_n, C_n, B_n and D_n are real functions for real refractive index m. Their explicit form has been given elsewhere (Chýlek, 1973).

For simplicity of discussion we consider a real index of refraction m. Then it follows that the $Re\{a_n\}$ and $Re\{b_n\}$ reach a series of absolute maxima $Re\{a_n\} = 1$ and/or $Re\{b_n\} = 1$ at such values of x ($x = 2\pi r/\lambda$ is a size parameter) where $Im\{a_n\} = 0$ and/or $Im\{b_n\} = 0$. At sufficiently high values of n, the first maximum in each partial wave amplitude a_n and b_n has the form of a sharp peak. In Figures 1A and 1B the first peaks in $Re\{a_{10}\}$ and $Re\{a_{20}\}$ are shown, and Figures 2A and 2B show the first sharp peak in $Re\{b_{31}\}$ as well as $Im\{b_{31}\}$. These sharp peaks we call resonances. We notice that with increasing n the first peak in each partial wave becomes narrower; also with an increasing value of refractive index m the peaks become narrower. At higher values of n not only the first peak but also a few of the following peaks may be sharp enough to be called resonances.

2. WHAT ARE SURFACE WAVES?

There seems to be no generally accepted definition of what is a surface wave in the case of scattering of electromagnetic waves on small particles. We are going to define what we mean by a surface wave. We have no intention in claiming that our definition should be generally accepted. We simply feel that since we deal with surface waves, we have to define clearly what is meant by it in this paper.

We make a reference to the two well-known phenomena generally attributed to surface waves, namely the ripple structure of the extinction cross section (Fig. 3A) and to the glory phenomena of backscattering (Fig. 3B). From a large number of published papers and from available monographs on light scattering we can learn that the ripple structure in the extinction cross section is presumably caused by the interference phenomena between a forward diffracted wave and the surface wave. Similarly the peaks appearing in the backscattering cross section (glory) are supposed to be a result of interference between the backward reflected wave and the surface wave. Without trying to discuss the validity of the above statements, we will show that both the ripple structure of extinction cross section and the glory in the backscattering are caused by the previously described resonances in the partial wave amplitudes a_n and b_n.

Let us go back to Figures 2A, 3A and 3B. We notice that the resonance in b_{31} (Fig. 2A) occurs somewhere between $26.9 < x < 27.0$. We also notice that in the same region of x there appears a sharp peak in the ripple structure (Fig. 3A) and a glory (sharp peak) in the backscattering cross section (Fig. 3B). This leads to a conjecture, suggested some time ago by one of the authors, that there is one-to-one correspondence between the partial wave resonances and the ripple structure in the extinction and the glory in the backscattering.

FIG. 1A. The first resonance in the partial wave a_{10} occurs at $x = 9.203$ for refractive index $m = 1.50$.

FIG. 1B. With increasing n the resonances become narrower. The first resonance in a_{20} occurs at $x = 16.65$.

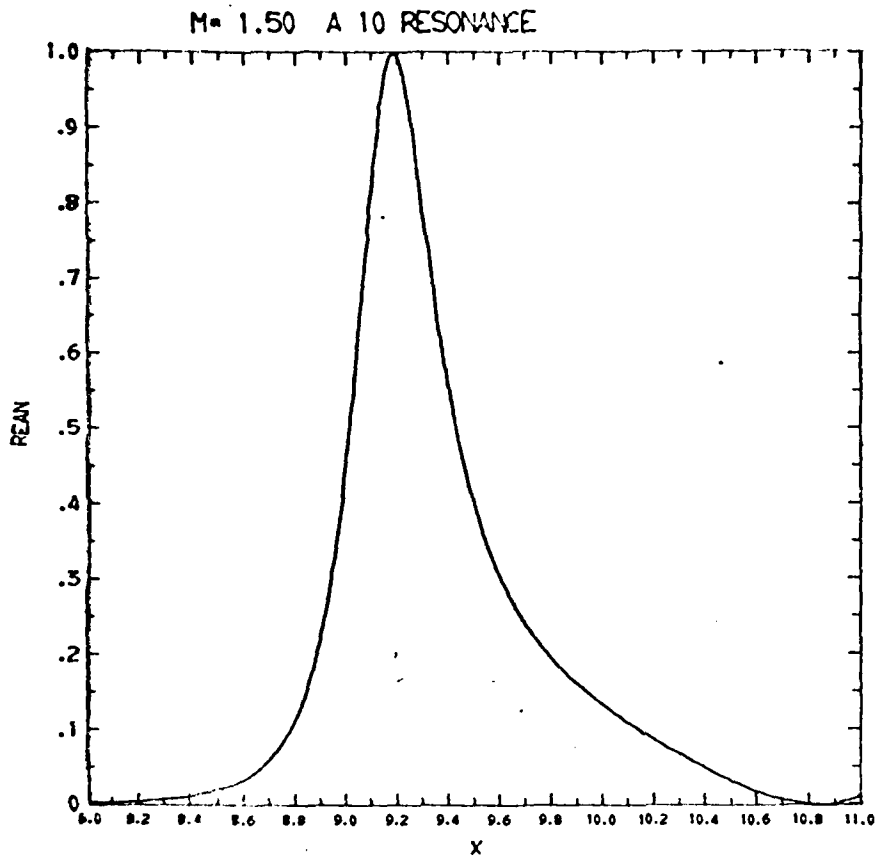
M= 1.50 A 10 RESONANCE
REAN
X
1.0
.9
.8
.7
.6
.5
.4
.3
.2
.1
0
8.0 8.2 8.4 8.6 8.8 9.0 9.2 9.4 9.6 9.8 10.0 10.2 10.4 10.6 10.8 11.0

12

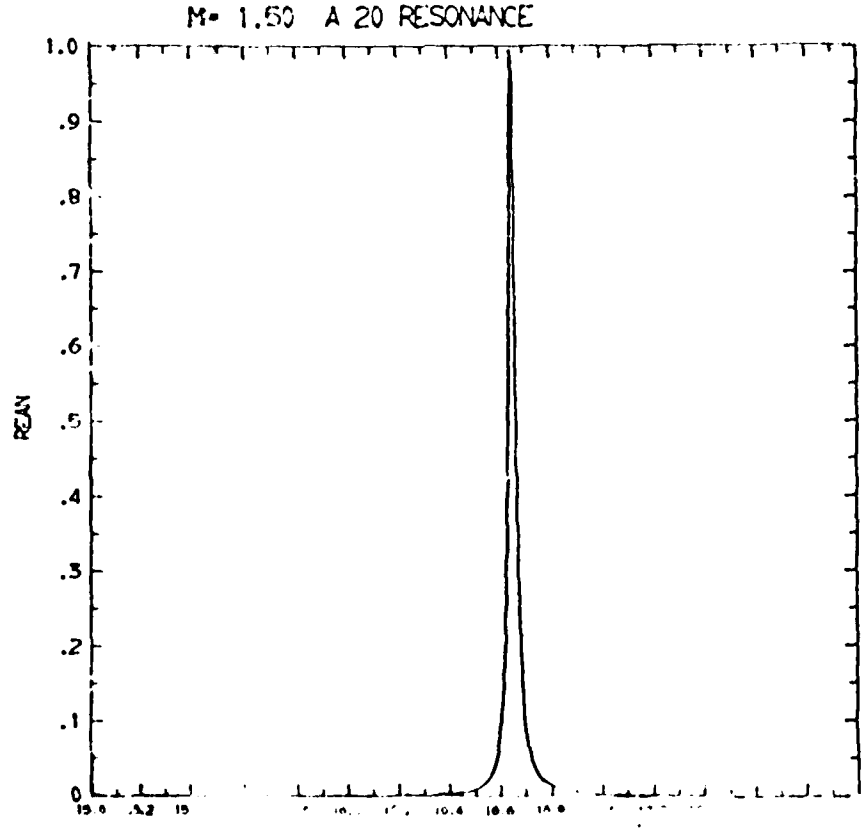
M= 1.50 A 20 RESONANCE
REAN
1.0
.9
.8
.7
.6
.5
.4
.3
.2
.1
0

13

FIG. 2A. In general the a_n resonances are sharper than the b_n resonances of the same value of n. Also, with higher refractive index m, resonances are narrower. The first resonance in b_{31} for refractive index m = 1.33 has a width comparable to the width of a_{20} (with m = 1.50).

FIG. 2B. The imaginary part of b_{31} goes through a zero in the direction from positive to negative values at the x value at which the real part of b_{31} reaches its maximum value $Re\{b_{31}\} = 1$.

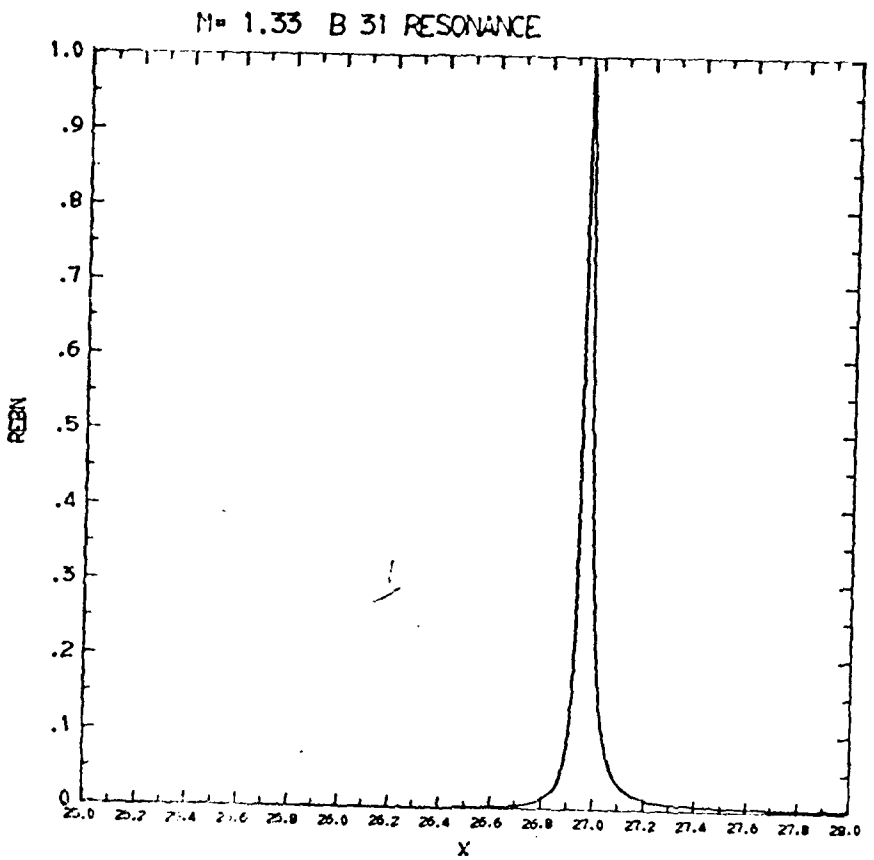
M= 1.33 B 31 RESONANCE
REBN
X

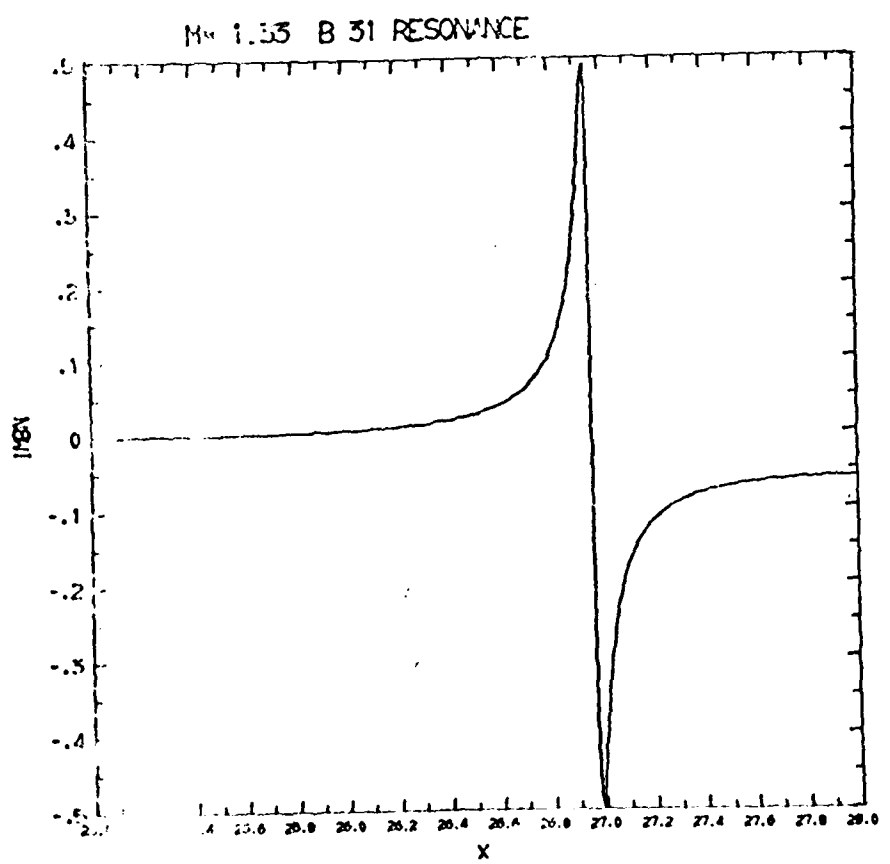
M= 1.33 B 31 RESONANCE
IMBN
X

FIG. 3A. The normalized extinction cross section Q_{EXT} (efficiency for extinction) shows a ripple structure. Each peak in a ripple corresponds to a definite resonance in the partial waves a_n or b_n (surface waves). The peak between $26.9 < x < 27.0$ corresponds to the b_{31} resonance.

FIG. 3B. The backscattering is completely dominated by the surface waves (partial wave resonances in a_n and b_n). Again the peak in the backscattering between $26.9 < x < 27.0$ is caused by the first resonance in the b_{31} partial wave.

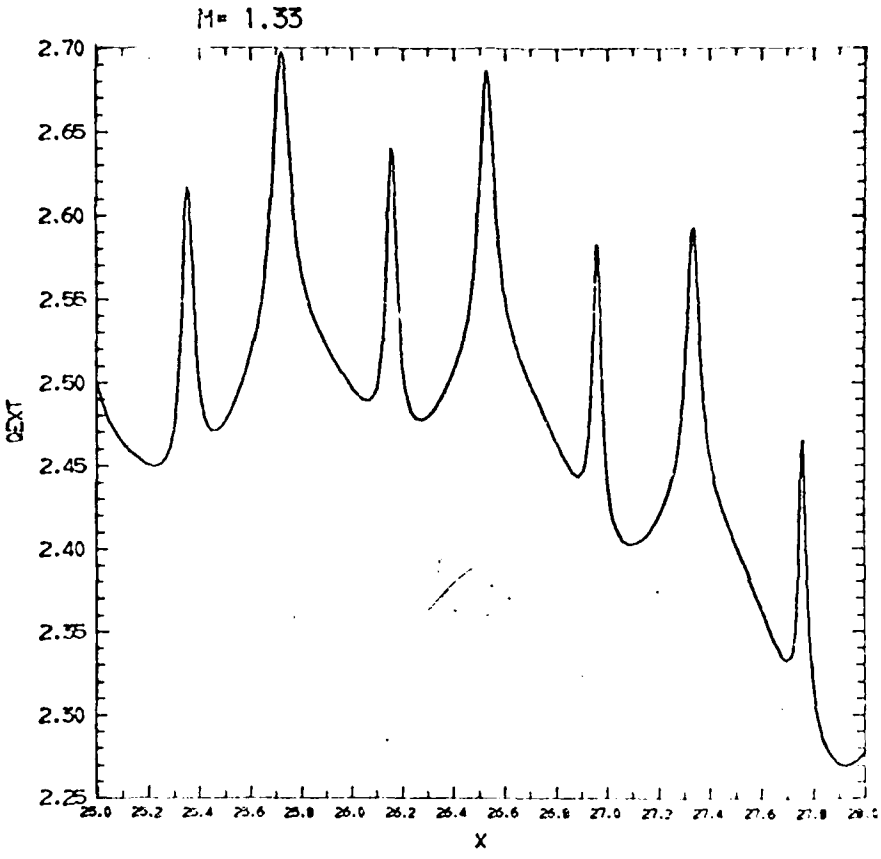
M= 1.33
QEXT
X

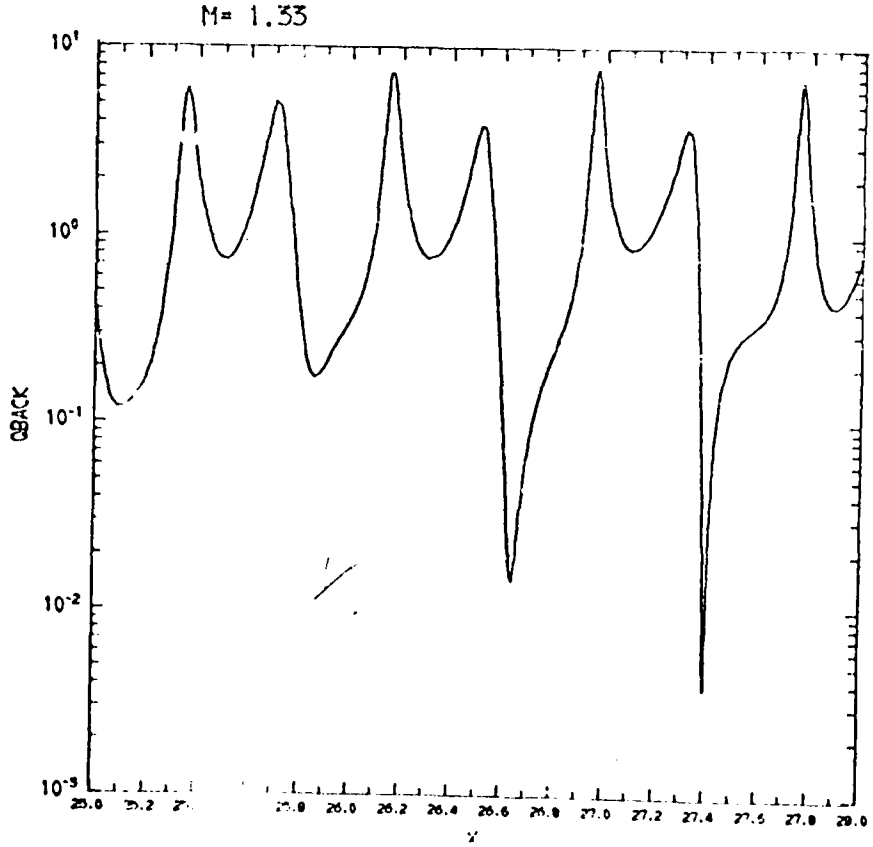
M= 1.33
QBACK
Y

[illegible] correct, when we remove the resonance from the Mie [illegible] $\zeta_{31} b_{31} = 0$ in the resonance region $26.6 < x < 28.0$) we expect the peak in extinction and the glory in the back scattering at $26.9 < x < 27.0$ to disappear. The results are shown in Figures 4A and 4B. Comparing Figure 3A with 4A and Figure 3B with 4B shows clearly that the peak in the ripple structure of the extinction wave between $26.9 < x < 27.0$ and the glory in the back scattering in the same x region is caused by nothing else than the resonance in the partial wave amplitude b_{31} (Fig. 2A).

Since, as we have mentioned earlier, both the ripple and the glory are supposed to be caused by surface waves, and since we have shown that they are caused by nothing else than the resonances in the partial waves a_n and b_n, we will say that the resonances in the partial waves a_n and b_n represent a mathematical description of surface waves.

At higher values of x, it is possible that more than one partial wave resonates at the same value of x. Then we may say that the surface wave is a kind of collective phenomenon arising from several partial waves resonating at the same size parameter x, as we have suggested earlier (Chýlek, 1976).

At the same time, we have to realize that there is a rather subjective judgment to decide when the width of a peak is narrow enough for a peak to be called a resonance.

3. RESONANCE AND BACKGROUND CONTRIBUTION TO THE EXTINCTION CURVE

The value of the extinction at the peak of the ripple structure can be decomposed into two parts; the resonance contribution and the background contribution:

$$Q_{EXT}(x) = Q_{EXT,RES}(x) + Q_{EXT,B}(x) \quad \text{where} \tag{2}$$

$$Q_{EXT,RES}(x) = \frac{2}{x^2} (2N + 1) \mathrm{Re}\{a_N(x)\} = \frac{2}{x^2} (2N + 1), \tag{3}$$

$$Q_{EXT,B}(x) = \frac{2}{x^2} \sum_{n=1}^{\infty}{}' (2n + 1) \mathrm{Re}\{(a_n + b_n)\}. \tag{4}$$

We assume that it is the partial wave $a_N(x)$ that resonates at the considered value of x, and the symbol $\sum'$ means the sum over all contributing a_n and b_n amplitudes with the exception of the resonating wave a_N.

FIG. 4A. To demonstrate that the ripple structure of the extinction curve is caused by the partial wave resonances in a_n and b_n, we have calculated again Q_{EXT}, however, now we have set $b_{31} = 0$ in the resonance region $26.6 < x < 27.4$. Comparing Figs. 3A and 4A we notice that the peak in Q_{EXT} between $26.9 < x < 27.0$ disappears, which shows clearly that the peak is formed by the b_{31} resonance.

FIG. 4B. When the b_{31} resonance is removed from the backscattering calculation the peak in the backscattering (glory) between $26.9 < x < 27.0$ disappears, which shows that the peak is formed by the b_{31} resonance.

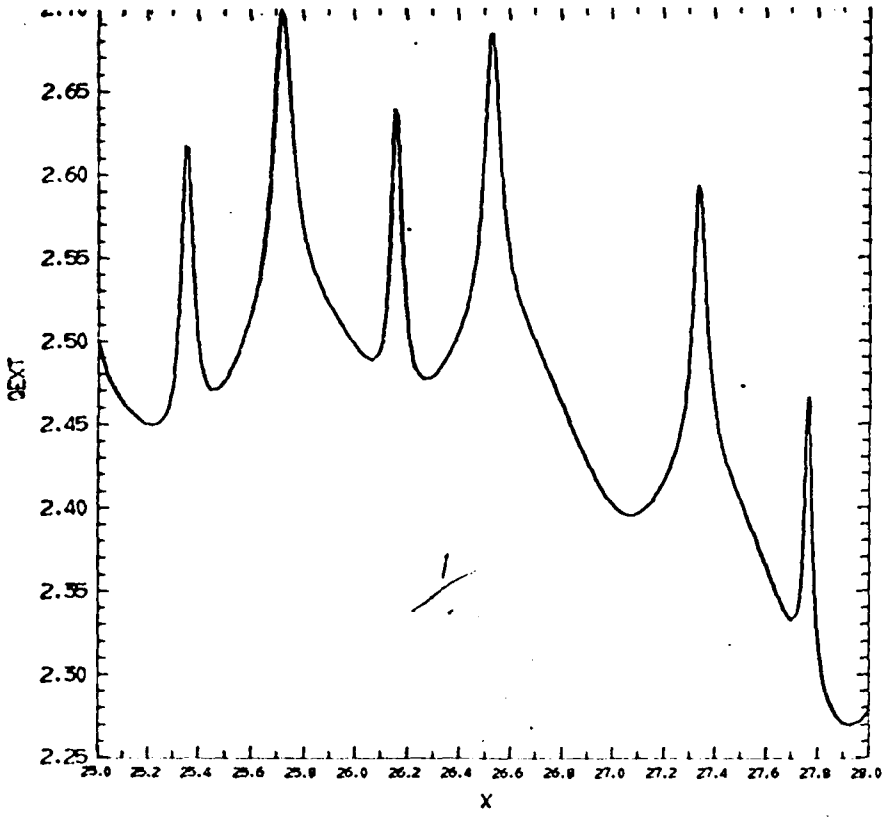
2.65
2.60
2.55
2.50
2.45
2.40
2.35
2.30
2.25
2EXT
25.0 25.2 25.4 25.6 25.8 26.0 26.2 26.4 26.6 26.8 27.0 27.2 27.4 27.6 27.8 28.0
X

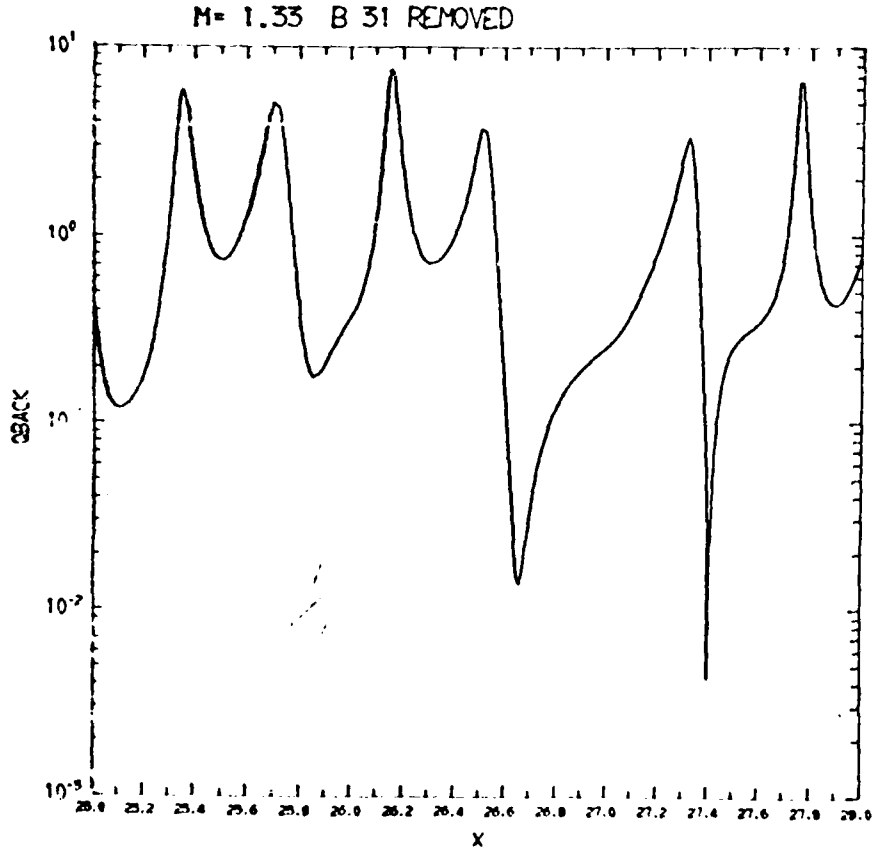
M= 1.33 B 31 REMOVED
10¹
10⁰
10⁻²
2BACK
25.0 25.2 25.4 25.6 25.8 26.0 26.2 26.4 26.6 26.8 27.0 27.2 27.4 27.6 27.8 28.0
X

Let us consider the resonance contributions of $a_{10}(x)$ and $a_{20}(x)$. The peak of the extinction curve at $x = 9.203$ (Fig. 5A) corresponds to the a_{10} resonance and the peak at $x = 16.65$ (Fig. 6A) corresponds to the a_{20} resonance. Using Equation (4) we can calculate the background contributions (see Fig. 5B and 6B) and we obtain $Q_{EXT,B}(9.203) = 1.982$, $Q_{EXT,B}(16.65) = 2.502$. Subtracting the values from the extinctions, $Q_{EXT}(9.203) = 2.475$ and $Q_{EXT}(16.65) = 2.798$, we obtain for the resonance contributions $Q_{EXT,RES}(9.203) = 0.493$ and $Q_{EXT,RES}(16.65) = 0.296$ or, in the form of a ratio of the a_{20} and a_{10} resonance contributions, we obtain

$$\frac{Q_{EXT,RES}(16.65)}{Q_{EXT,RES}(9.203)} = 0.600 .$$

If we calculate the ratio of the same resonance contributions using an approximate form of equation (3) we obtain

$$\frac{Q_{EXT,RES}(16.65)}{Q_{EXT,RES}(9.203)} = \frac{41\ (9.203)^2}{21\ (16.65)^2} = 0.596 ,$$

in excellent agreement with the previously obtained value of 0.600.

We conclude that the resonance or surface wave contribution to the extinction described by equation (3) is in agreement with numerical results.

4. SURFACE WAVES IN EXPERIMENTAL MEASUREMENTS

Recently a technique of optical levitation was used to support a liquid droplet in a laser beam (Ashkin, 1970; Ashkin and Dziedzic, 1976, 1977). One of the authors (A. Ashkin) used this technique in connection with a tunable laser to measure the backscattering. An example of the measurement of the backscattered intensity is shown in Figure 7a. Three strong peaks observed in the wavelength interval correspond to the glory effect. Since the droplet radius is known only approximately it is not possible to label the horizontal axis in size parameter units at this time.

The first point we want to demonstrate is that there is only one way to identify the experimental measurement with theoretical calculations when the droplet radius is essentially unknown. The results of the backscattering calculations with the size parameter increment of $\Delta x = 0.001$ are shown in Figure 7b. We notice how the sharp resonance (glory) is superimposed on a broader background (really of the same background coming from the terms with $n < x$ plus

FIG. 5A. The normalized extinction cross section Q_{EXT} is composed from the resonance contributions superimposed on the background term.

FIG. 5B. When the first a_{10} resonance is removed around x = 9.2 only the background term remains.

5a

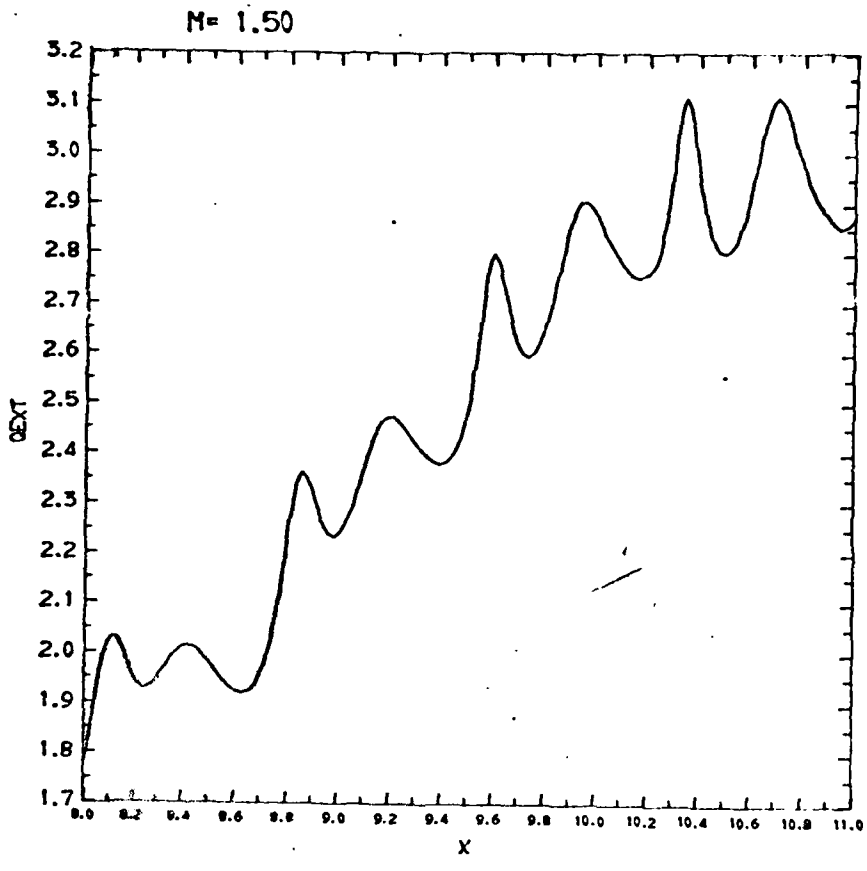
M= 1.50
QEXT
X
3.2
3.1
3.0
2.9
2.8
2.7
2.6
2.5
2.4
2.3
2.2
2.1
2.0
1.9
1.8
1.7
8.0
8.2
8.4
8.6
8.8
9.0
9.2
9.4
9.6
9.8
10.0
10.2
10.4
10.6
10.8
11.0

5b

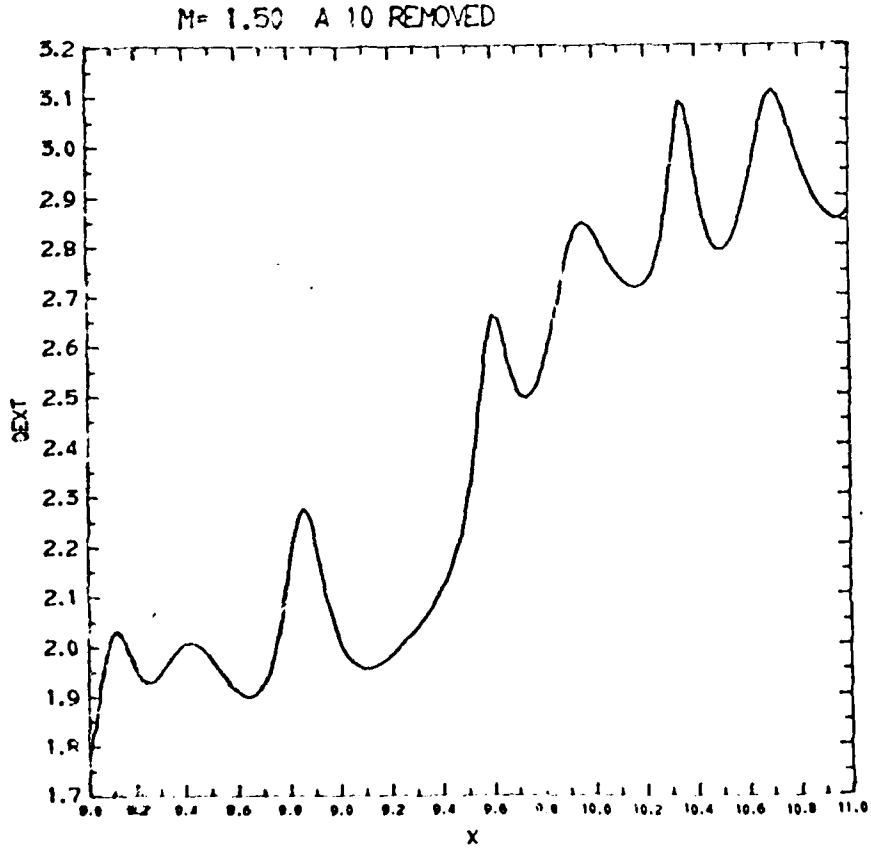
M= 1.50 A 10 REMOVED
QEXT
X
3.2
3.1
3.0
2.9
2.8
2.7
2.6
2.5
2.4
2.3
2.2
2.1
2.0
1.9
1.8
1.7
8.0
8.2
8.4
8.6
8.8
9.0
9.2
9.4
9.6
9.8
10.0
10.2
10.4
10.6
10.8
11.0

FIG. 6A. The peak in Q_{EXT} around x = 16.6 is caused by the a_{20} resonance.

FIG. 6B. When the a_{20} resonance is removed from the calculations (we set a_{20} = 0) the peak around x = 16.6 disappears and only the background term is left.

6a

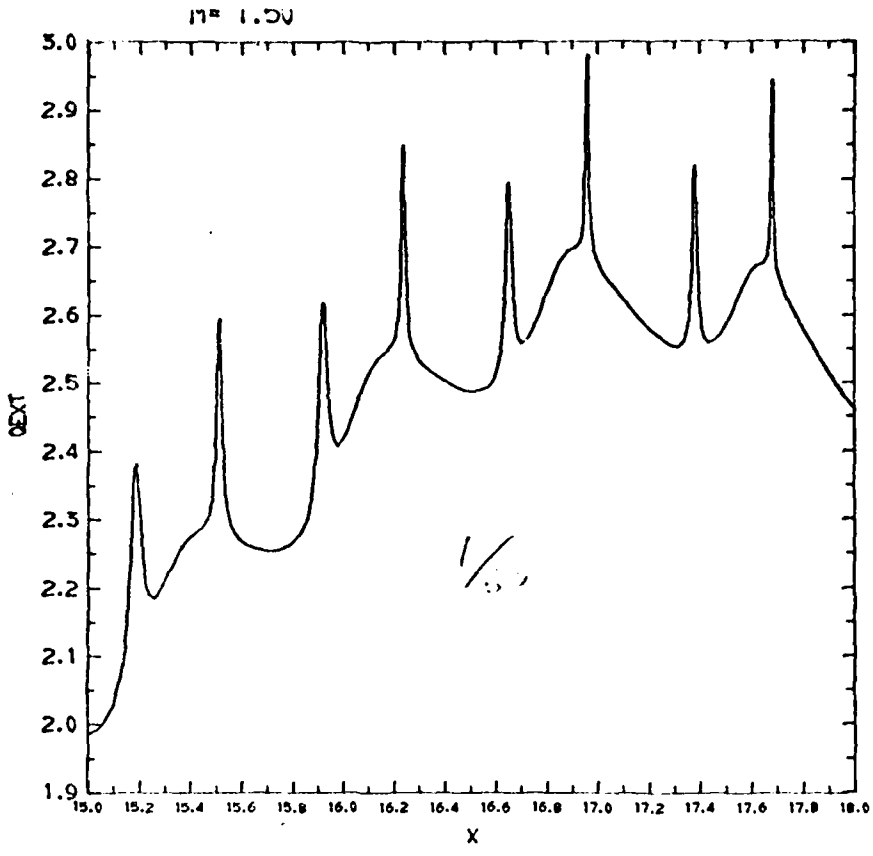
M= 1.50
3.0
2.9
2.8
2.7
2.6
2.5
2.4
2.3
2.2
2.1
2.0
1.9
QEXT
15.0 15.2 15.4 15.6 15.8 16.0 16.2 16.4 16.6 16.8 17.0 17.2 17.4 17.6 17.8 18.0
X

6b

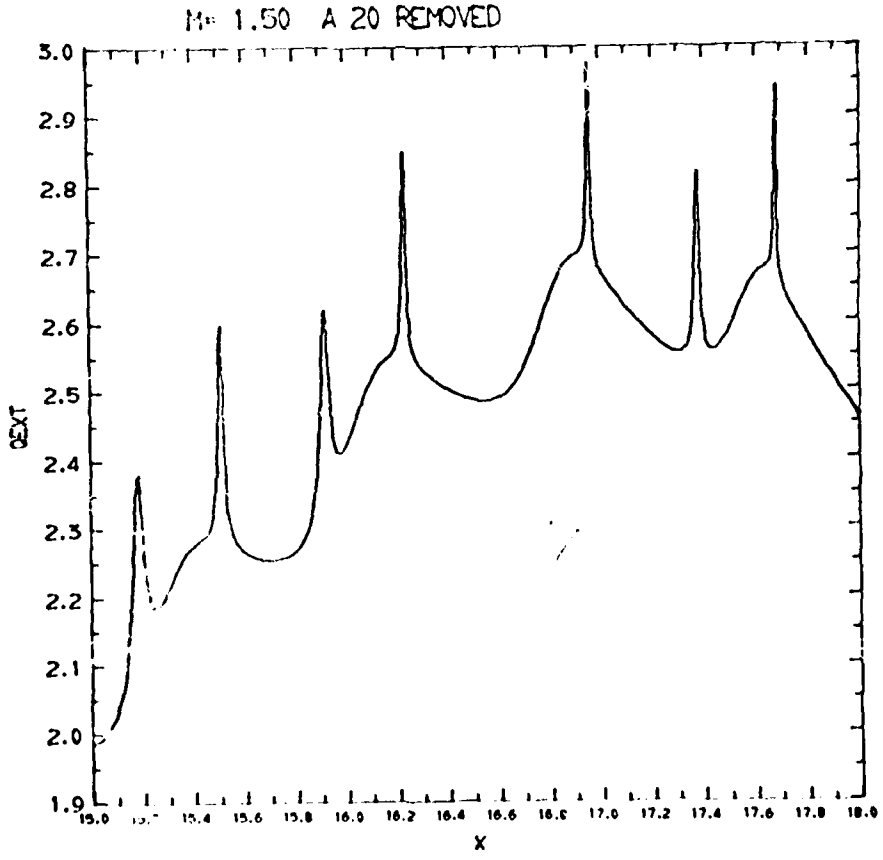
M= 1.50 A 20 REMOVED
3.0
2.9
2.8
2.7
2.6
2.5
2.4
2.3
2.2
2.1
2.0
1.9
QEXT
15.0 15.4 15.6 15.8 16.0 16.2 16.4 16.6 16.8 17.0 17.2 17.4 17.6 17.8 18.0
X

FIGS. 7A-7C. The experimental measurement (A) of the backscattering shows resonances superimposed upon the background. We notice narrow resonance peaks as well as the higher order broader resonances. The distance between the neighboring resonances of the same order depends slightly on the order of resonances and on the size parameter. Because of that, each group of resonances (denoted by 1, 2 and 3) has a different characteristic structure, *i.e.*, different morphology. The same structure appears in a coarse numerical calculation (B), and it is just this characteristic morphological structure of each group of resonances which allows us unambiguously to identify the experimentally observed peaks. A detailed numerical calculation (C) reveals additional narrow resonances that have not been observed experimentally because their width is below the resolution power of the experimental equipment used. The refractive index of oil droplet used is m = 1.42.

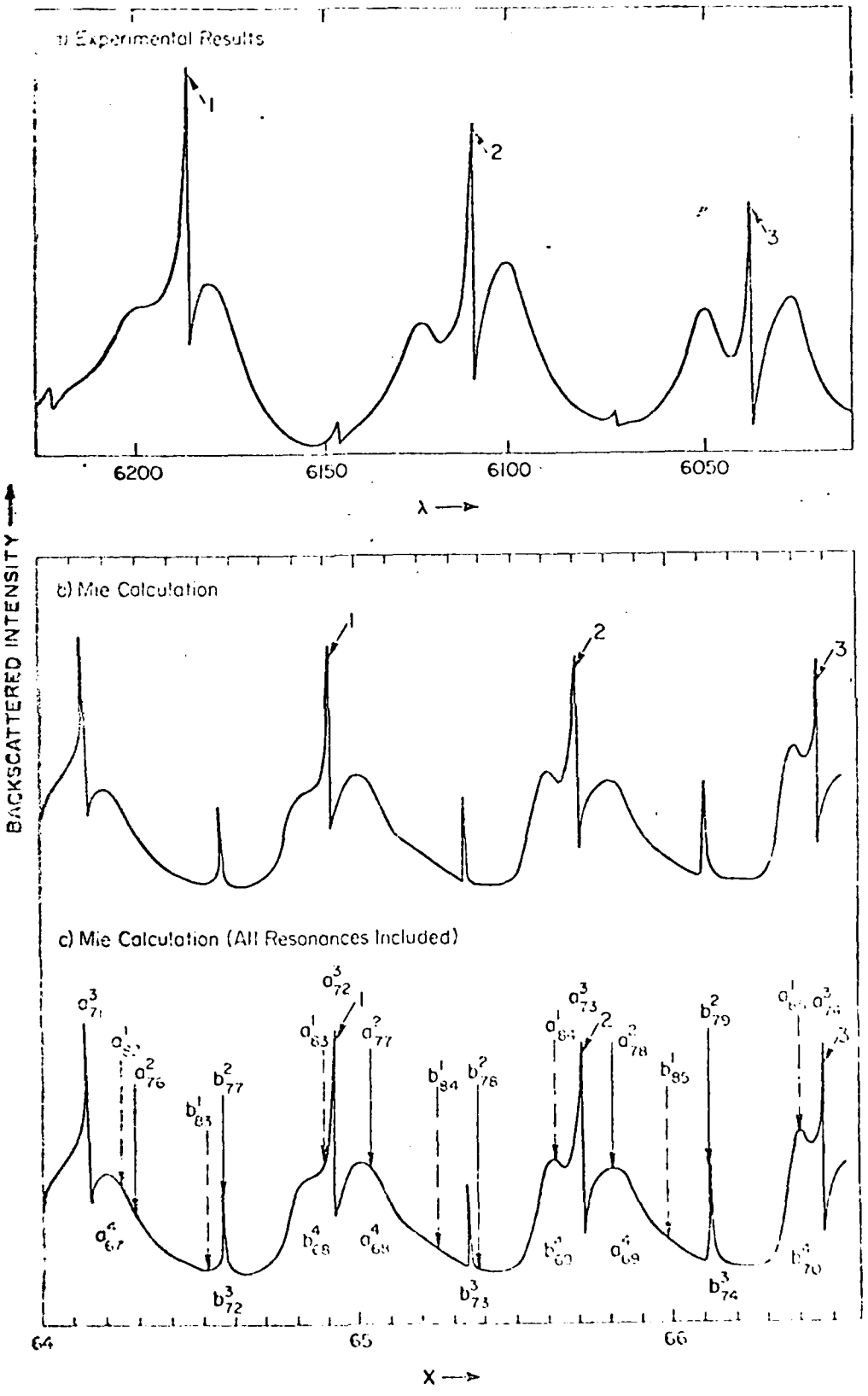
a) Experimental Results
1
2
3
6200
6150
6100
6050
λ
BACKSCATTERED INTENSITY
b) Mie Calculation
c) Mie Calculation (All Resonances Included)
64
65
66
X

Fig. 7

a broader higher order resonances in partial waves with n ≈ x). We conclude that the morphology of the resonance structure leads to an unambigous identification of the experimentally measured peak 1 in Figure 7A with the theoretically calculated peak 1 in Figure 7B. Now, since we know precisely the wavelength λ at which peak 1 was observed as well as the size parameter x at which peak 1 occurs in the numerical calculations, we can determine with a high degree of accuracy the radius of the observed droplet, as has been already demonstrated elsewhere (Chýlek *et al.*, 1978a, 1978b).

We were fully aware that by using the step size of $\Delta x = 0.001$ in our numerical calculations we could lose many of the narrow peaks in the backscattering structure. By using a computer resolution of the same order as the resolution of the experimental equipment used, we hoped to get comparable structures as shown in Figures 7A and 7B. By increasing the resolution of our numerical calculations we obtain the full backscattering structure (Fig. 7C). It follows that the resolution power of the instrumental arrangement used was not high enough to observe the first and the second order resonances. To observe these narrow resonances the resolution power of experimental observation has to be increased by several orders of magnitude.

5. SURFACE WAVES ON NON-SPHERICAL PARTICLES

Our preliminary results indicate that surface waves do exist at least in definite orientations of axially symmetric non-spherical particles. On the other hand, the strength of surface waves is considerably reduced when non-spherical particles are in random orientation. These conclusions were deduced from numerical calculations using the extended boundary condition method. Details of these calculations will be reported elsewhere.

Acknowledgments. The research was partially supported by the U.S. Army Research Office and the Atmospheric Research Section of the National Science Foundation. The National Center for Atmospheric Research is sponsored by the National Science Foundation.

REFERENCES

Ashkin, A., 1970, *Phys. Rev. Letters*, *24*, 156.
Ashkin, A. and Dziedzic, J. M., 1976, *Phys. Rev. Letters*, *36*, 267.
Ashkin, A. and Dziedzic, J. M., 1977, *Phys. Rev. Letters*, *38*, 1351.
Chýlek, P., 1973, *J. Opt. Soc. Am.*, *63*, 699.
Chýlek, P., 1976, *J. Opt. Soc. Am.*, *66*, 285.
Chýlek, P., Kiehl, J. and Ko, M., 1978a, *Phys. Rev.*, *A18*, 2229.
Chýlek, P., Kiehl, J. and Ko, M., 1978b, *Appl. Opt.*, *17*, 3019.